FERONIA controls pectin- and nitric oxidemediated male-female interaction

https://doi.org/10.1038/s41586-020-2106-2

Received: 7 November 2018

Accepted: 17 January 2020

Published online: 18 March 2020



Check for updates

Qiaohong Duan^{1,2,9}, Ming-Che James Liu^{1,3,9}, Daniel Kita^{1,4,7}, Samuel S. Jordan¹, Fang-Ling Jessica Yeh¹, Robert Yvon^{1,4}, Hunter Carpenter^{1,4}, Anthony N. Federico^{1,8}, Liliana E. Garcia-Valencia¹, Stephen J. Eyles^{1,5}, Co-Shine Wang³, Hen-Ming Wu^{1,4™} & Alice Y. Cheung^{1,4,5,6} ⊠

Species that propagate by sexual reproduction actively guard against the fertilization of an egg by multiple sperm (polyspermy). Flowering plants rely on pollen tubes to transport their immotile sperm to fertilize the female gametophytes inside ovules. In Arabidopsis, pollen tubes are guided by cysteine-rich chemoattractants to target the female gametophyte^{1,2}. The FERONIA receptor kinase has a dual role in ensuring sperm delivery and blocking polyspermy³. It has previously been reported that FERONIA generates a female gametophyte environment that is required for sperm release⁴. Here we show that FERONIA controls several functionally linked conditions to prevent the penetration of female gametophytes by multiple pollen tubes in Arabidopsis. We demonstrate that FERONIA is crucial for maintaining de-esterified pectin at the filiform apparatus, a region of the cell wall at the entrance to the female gametophyte. Pollen tube arrival at the ovule triggers the accumulation of nitric oxide at the filiform apparatus in a process that is dependent on FERONIA and mediated by de-esterified pectin. Nitric oxide nitrosates both precursor and mature forms of the chemoattractant LUREI¹, respectively blocking its secretion and interaction with its receptor, to suppress pollen tube attraction. Our results elucidate a mechanism controlled by FERONIA in which the arrival of the first pollen tube alters ovular conditions to disengage pollen tube attraction and prevent the approach and penetration of the female gametophyte by late-arriving pollen tubes, thus averting polyspermy.

The mechanisms that underlie the interplay between pollen and pistil—the male and female components, respectively—in flowering plants have been investigated for decades^{5,6}. From the receptive surface of the pistil, a pollen grain extrudes a tube to transport sperm to the female gametophyte for fertilization (Fig. 1a). Pollen tubes grow in the transmitting tissue and along the ovule surface (Extended Data Fig. 1a) in an extracellular matrix enriched in glycosylated molecules^{7,8}. These tubes depart from their main growth axis and, in response to guidance cues from the female, each targets an ovule and penetrates a synergid cell at the entrance of the female gametophyte, upon which the pollen tube bursts and releases sperm. Occurrences in which multiple pollen tubes penetrate a female gametophyte are rare, even when pollen tubes are plentiful; tubes that arrive late bypass pollinated ovules to target those that are not yet pollinated, thus averting polyspermy while maximizing reproductive yield. The synergid cells secrete chemoattractants, such as the cysteine-rich peptides LUREs¹ and their homologues $XIUQIUs^2, to guide pollen tubes to the female game to phyte {}^{1,2,5,6} (Fig. 1a).\\$ Once a pollen tube enters the female gametophyte, multiple factors are involved in ensuring reproductive success, in which FERONIA receptor kinase (FER) has a key role^{3,4,9}. In fer mutants, over 80% of the female gametophytes do not induce pollen tube rupture and about half are penetrated by multiple tubes, resulting in a pile-up of over-grown pollen tubes (Fig. 1b, c, Extended Data Fig. 1c). FER controls RHO GTPase signalling¹⁰ to generate a reactive oxygen species maximum at the filiform apparatus¹¹ to induce the rupture of the just-penetrated pollen tube and therefore sperm release⁴. How FER switches from this first act of enabling fertilization to a second act of blocking late-arriving pollen tubes has remained unclear.

The FER-controlled pollen tube block

To gain insight into how FER blocks supernumerary pollen tubes from entering the female gametophyte, we first examined when the mechanism is engaged. FER is broadly expressed, including in the sporophytic tissues of pistils^{4,10} (Extended Data Fig. 1b). Pollen tubes normally exit the transmitting track one at a time (Fig. 1b, Extended Data Fig. 1a), and fewer than 5% of wild-type ovules are penetrated by multiple pollen tubes (Fig. 1c, Extended Data Fig. 1c). In fer pistils, pollen tubes

Department of Biochemistry and Molecular Biology, University of Massachusetts, Amherst, MA, USA. 2State Key Laboratory of Crop Biology, College of Horticulture Science and Engineering, Shandong Agricultural University, Tai'an, China. 3 Graduate Institute of Biotechnology, National Chung Hsing University, Taichung, Taiwan. 4 Molecular and Cellular Biology Program, University of Massachusetts, Amherst, MA, USA, 5 Institute for Applied Life Sciences, Mass Spectrometry Center, University of Massachusetts, Amherst, MA, USA, 6 Plant Biology Graduate Program, University of Massachusetts, Amherst, MA, USA. ⁷Present address: Alexion Pharmaceutical Inc., New Haven, CT, USA. ⁸Present address: Bioinformatics Department, Boston University, Boston, MA, USA. ⁹These authors contributed equally: Qiaohong Duan, Ming-Che James Liu. ⁵²e-mail: hmwu@biochem.umass.edu; acheung@biochem.umass.edu

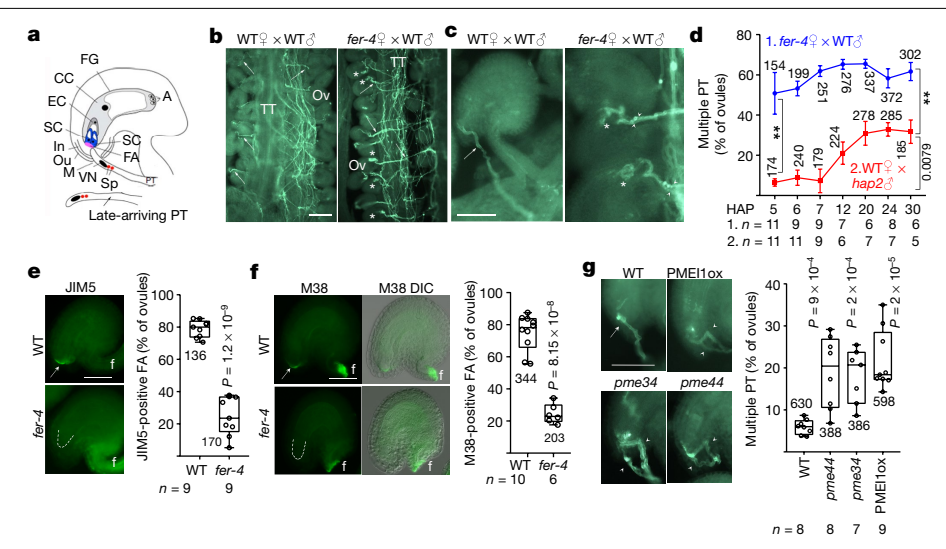


Fig. 1| The FER-mediated presence of de-esterified pectin underlies prevention of the entrance of supernumerary pollen tubes into ovules. a, An ovule cartoon. A, antipodal cells; CC, central cells; EC, egg cells; FA, filiform apparatus; FG, female gametophyte; In, inner integument; M, micropyle; Ou, outer integument; PT, pollen tube; SC, synergid cells; Sp, sperm; VN, vegetative nucleus. **b**, **c**, fer-4^{4,9,10} mutation induces defects in the interaction between pollen tubes and oyules. Pistils were pollinated by wild-type (WT) pollen. stained with aniline blue to show pollen tubes in transmitting tissue (TT) and penetrated ovules (Ov) (b). Asterisks in b, c indicate overgrowth of pollen tubes. Observations shown here were typical^{4,10}, and the analysis was repeated a total of six times for these experiments (and those shown in Extended Data Fig. 4). d, fer-4 mutation-induced multiple pollen tube entrance and hap2induced polytubey. The fer-4 plant was pollinated by wild type (experiment 1), and wild type was pollinated by a hap2/+ plant (experiment 2). Typically, about 30% of ovules were penetrated at around 5 h after pollination (HAP), and increased to completion (about 90-100% of all ovules) by around 20 h after

pollination. In experiment 2, 50% of hap2/+ pollen did not fertilize^{12,13}. Data shown are average \pm s.e.m. *n* indicates the number of pistils. **P< 0.01 (for example, 0.0019 for 5 h after pollination, 0.002 for 30 h after pollination). \mathbf{e} , \mathbf{f} , Immunodetection of ovular de-esterified pectin by JIM5 (\mathbf{e}) and M38 (\mathbf{f})^{18,28}. Dashed lines, micropylar ends. Data shown are average \pm s.d. n indicates the number of pistils. g, Phenotype of pollen tube entrance in wild-type pme34, $pme44^{29,30}$ and PMEI1ox oyules. Data shown are average \pm s.d. n indicates the number of pistils. P values were obtained by two-tailed t-tests; numbers in data plots denote the number of ovules examined. Data in $\mathbf{d} - \mathbf{g}$ are representative of three independent experiments. Scale bars, $50 \, \mu m \, (\mathbf{c}, \mathbf{e} - \mathbf{g})$, $100 \, \mu m \, (\mathbf{b})$. Arrows indicate pollen tube exit from the transmitting tissue to target ovules in b, single pollen tube entrance into an ovule in c, g and filiform apparatus in e, f; arrowheads in c, g indicate multiple pollen tube entrance into an ovule; f in e, findicates funiculus autofluorescence. Box plots: centre line, median; box limits, lower and upper quartiles; dots, individual data points; whiskers, highest and lowest data points.

exited the transmitting track in bundles (Fig. 1b). Between about 5 h after pollination (when pollen tubes began reaching the ovules) and the completion of fertilization at about 20 h after pollination, ≥50% of penetrated ovules received multiple pollen tubes (Fig. 1c, d, Extended Data Fig. 1c), which implies that the FER-mediated mechanism is constitutively engaged to suppress the entry of multiple pollen tubes. Several previous studies have demonstrated a phenomenon termed 'polytubey' in ovules that are penetrated but not fertilized¹²⁻¹⁴. Polytubey approximates the multiple pollen tube phenotype in fer-4 ovules, but is a result of a mechanism called 'fertilization recovery' that is enacted to salvage fertilization. When pistils were pollinated by pollen from hap2/+ mutant plants^{12,13}, half of the pollen did not fertilize and we observed that polytubey occurred starting only at around 7–8 h after pollination (Fig. 1d)—at which time the earliest-arrived pollen tubes should have already accomplished fertilization. The comparison here therefore provides a clear contrast between the FER-mediated mechanism that actively and constitutively blocks the penetration of ovules by supernumerary pollen tubes and the polytubey phenomenon that is induced by fertilization recovery.

FER regulates ovular pectin

Several considerations guided our investigation into how FER suppresses polyspermy, including the fact that pollen tube growth is extracellular and the two related observations that the extracellular domain of FER binds pectin¹⁵ (a complex carbohydrate that is important for the integrity of the cell wall¹⁶) and the loss of FER weakens the cell wall¹⁵. Ruthenium red (which binds demethylesterified pectin (homogalacturonan)¹⁷) and the antibodies JIM5 and M38 (which recognize partially

and fully de-esterified pectins, respectively¹⁸) all detected a significant reduction in de-esterified pectins at the filiform apparatus of *fer-4* ovules relative to wild type (Fig. 1e, f, Extended Data Fig. 1d–h). FER is prominently located at the filiform apparatus⁴ (Extended Data Fig. 1b), which is densely populated by the synergid cell membrane¹¹. It is plausible that the interaction between FER and pectin¹⁵ at the wall–membrane interface stabilizes the association of pectin with the wall matrix.

We then explored whether FER-regulated pectin was associated with the FER-mediated mechanism to block the entrance of multiple pollen tubes. In planta, pectin is secreted as methylesterified homogalacturonan and is de-esterified by pectin methylesterases (PMEs) located in the cell wall. This modification exposes carboxyl groups for crosslinking by divalent cations (such as Ca²⁺ in the wall matrix) and rigidifies the wall¹⁶. The level of pectin de-esterification is carefully guarded. For example, the Arabidopsis genome has 66 PMEs and 69 putative PME inhibitors (PMEIs) that together regulate levels of methylesterified and de-esterified pectins, rendering genetic manipulation of pectin homeostasis extremely challenging^{19,20}. To compromise the ovular pectin condition, we identified mutants in the ovule-expressed PME34 and PME44 genes and generated PMEI1 overexpression lines (PMEI1ox) (Extended Data Fig. 2a-g). These plants were relatively normal, but their ovules showed reduced levels of de-esterified pectin in the filiform apparatus and more entries of multiple pollen tubes than in wild type (Fig. 1g, Extended Data Figs. 1i, j, 2l). Taken together with observations in *fer* ovules (Fig. 1e, f), our results are consistent with the FER-mediated presence of deesterified pectin at the filiform apparatus being associated with the mechanism to prevent the entry of supernumerary pollen tubes into the female gametophyte.

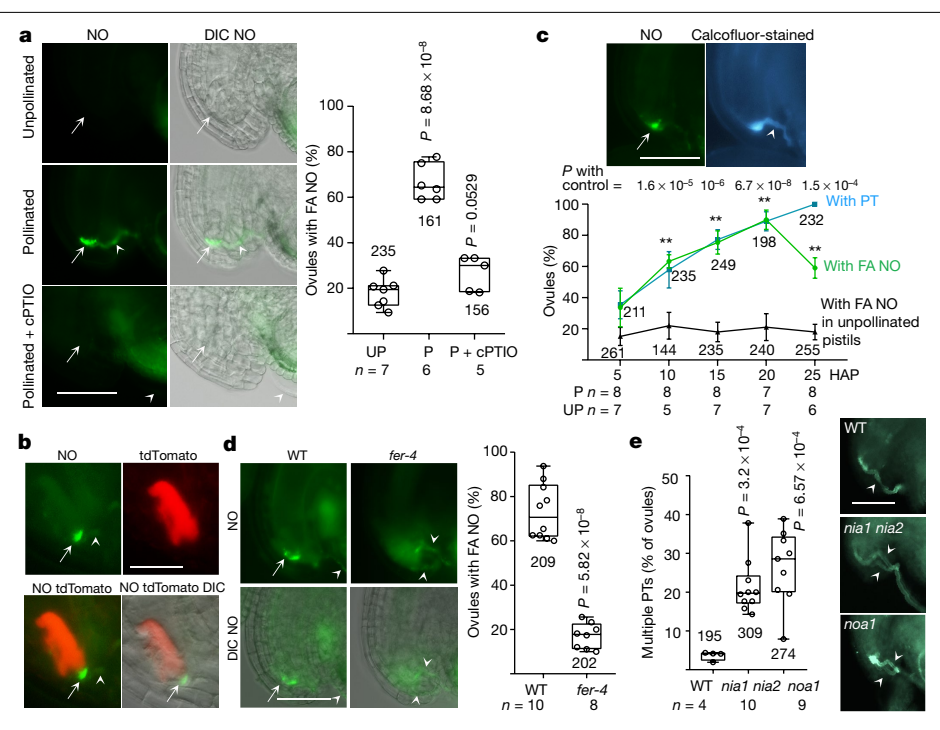


Fig. 2 | Pollination induces FER-dependent NO at the filiform apparatus. a, b, Ovular NO. a, Ovules from unpollinated (UP) and pollinated (P) wild-type pistils collected 18 hafter pollination, stained by 4,5-diaminofluorescein $diacetate\,(DAF\text{-}DA)\,with\,or\,without\,the\,NO\,scavenger\,cPTIO^{22,23,31,32}.\,Data$ shown are average \pm s.d. **b**. A wild-type ovule penetrated by a tdTomatoexpressing pollen tube, stained by DAF-DA. Image is representative of more than 30 penetrated ovules from two independently pollinated pistils, carried out for the purpose of unambiguously demarcating the boundary between the synergid cells and the filiform apparatus. **c**, Filiform apparatus NO and pollen tube penetration. Ovules from unpollinated and pollinated pistils were stained

with DAF-DA to image NO, and then stained with calcofluor white for pollen

tubes. Data shown are average ± s.d. d, NO in wild-type and fer-4 ovules penetrated by pollen tubes. Data shown are average ± s.d. e, Phenotype of pollen tube entrance in NO-deficient nia1 nia2 and noa1 ovules 33-36. Data shown are average \pm s.d. *P* values by two-tailed *t*-tests. Data in **a**, **c**-**e** are representative of three independent experiments. DIC. differential interference contrast. Scale bars, 50 µm. Arrows indicate filiform apparatus; arrowheads indicate pollen tubes. In a, c-e, n denotes the number of pistils and numbers in the plots indicate total number of ovules examined. Box plots: centre line, median; box limits, lower and upper quartiles; dots, individual data points; whiskers, highest and lowest data points.

FER regulates ovular nitric oxide

We then explored whether there were other FER-regulated conditions involved in blocking the entry of multiple pollen tubes into ovules. Given that the FER-mediated reactive oxygen species maximum in the filiform apparatus region is important for pollen tube rupture⁴, and that reactive oxygen species and nitric oxide (NO) are engaged in intimate functional and signalling interplays (including regulating pollen tube growth and directional responses^{21,22}), we examined whether FER prevents the entrance of multiple pollen tubes by affecting ovular NO. Because the genetic manipulation of NO production in plants and its detection are inherently challenging²³, we followed previously established and often-used approaches 21-23 and observed that pollen tube arrival at the ovule induced NO accumulation at the filiform apparatus (Fig. 2a, b). During pollination, the increase in ovules that accumulated NO at the filiform apparatus was FER-dependent and paralleled the increase in penetrated ovules (Fig. 2c, d, Extended Data Fig. 3a-c). Ovules from the NO-deficient mutants nia1 nia2 and noa1 had reduced levels of filiform apparatus NO (Extended Data Fig. 3d) and increased multiple pollen tube entry relative to wild type (Fig. 2e), providing additional support for filiform apparatus NO being a factor in suppressing the entrance of supernumerary pollen tubes.

Pectin induces FER-dependent NO

Our observations thus far suggested that two FER-dependent conditions at the filiform apparatus—de-esterified pectin deposits and NO accululation induced by pollen tube arrival—were involved in guarding against polyspermy, and thus could be functionally linked. Pollen tubes produce copious amounts of enzymes related to cell wall metabolism, some of which degrade or modify pectin²⁴. We therefore examined how pollination might affect pectic constituents along the pollen tube growth pathway and whether FER has a role. Using JIM5 and M38, we detected a notable increase in de-esterified pectin in the exudate from pollinated wild-type pistils relative to its counterpart from unpollinated pistils, whereas fer-4 pistillate exudates lacked de-esterified pectin (Fig. 3a, Extended Data Fig. 4). Moreover, the pollinated wild-type exudate was active in stimulating the accumulation of filiform apparatus NO in ovules from unpollinated wild-type pistils (Fig. 3b), whereas exudates from fer-4 pistils lacked comparable activity (Extended Data Fig. 5a). Fragmented polygalacturonic acid (PGA) (Extended Data Fig. 5b) was also active in stimulating the accumulation of filiform apparatus NO, akin to the increase in NO triggered by oligogalacturonic acid in immunity signalling²⁵; fer-4 ovules were non-responsive (Fig. 3c, d, Extended Data Fig. 5c-e). PGA also stimulated NO accumulation in roots of wild-type-but not fer-4-seedlings (Fig. 3e, Extended Data Fig. 5f), which provides further support for a signalling linkage between de-esterified pectin, FER and increases in NO levels. Although the precise active species in the pistillate exudates and fragmented PGA remain unknown, observations here are consistent with pectic fragments generated by the growth of pollen tubes acting as signals to trigger NO accumulation at the filiform apparatus in a FER-dependent manner.

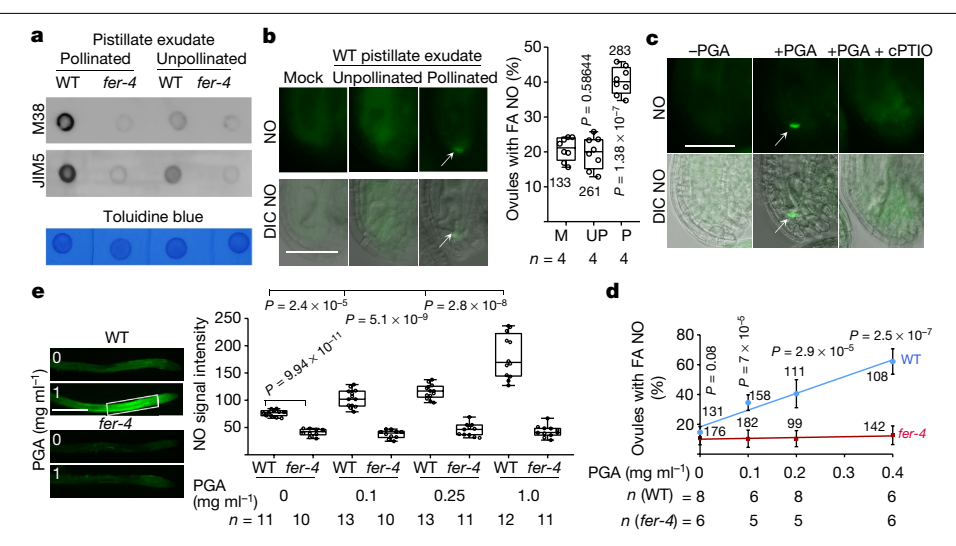


Fig. 3 | Pollinated pistil exudates and de-esterified pectin fragments induce FER-dependent NO. a, JIM5 and M38 immunodetection of de-esterified pectin in pistillate exudates. See Methods for exudate preparation. Two microlitres of (equivalent to 10 pistils) exudate was spotted for immunodetection. Toluidine-blue staining showed sample loading. Together with Extended Data Fig. 4, four independent preparations showed comparable results. **b**, Filiform apparatus NO induced by pistil exudate. Ovules were from unpollinated wild-type pistils; the ovules were mock (M)-treated or treated with 4 μ l exudates from unpollinated (UP) or pollinated (P) wild-type pistils (pollinated exudate had about 250 ng of JIM5-detected materials). Data shown are average \pm s.d., n = 4 replicates (2 pistils each). **c**, **d**, Filiform apparatus NO induced by fragmented PGA. **c**, Ovules were from unpollinated wild-type pistils and were

mock-treated (–PGA), or treated with PGA in the presence of cPTIO (1mM) or without cPTIO; all were stained by DAF-DA. $\bf d$, Ovular NO response to increasing PGA doses. Data shown are average \pm s.d. n indicates the number of pistils. $\bf e$, NO response to PGA in wild-type and fer-4 roots. Mock- or PGA (1mg ml $^{-1}$)-treated seedlings, stained with DAF-DA. Signals from identical areas (white box) were quantified. Data shown are average \pm s.d. n indicates the number of seedlings. P values were by two-tailed t-tests; numbers in data plots denote the ovules examined; data in $\bf b$, $\bf d$, $\bf e$ are representative of three independent experiments. Scale bars, 50 μ m. Arrows, filiform apparatus. Box plots: centre line, median; box limits, lower and upper quartiles; dots, individual data points; whiskers, highest and lowest data points.

Nitrosation inhibits LURE activity

In considering how NO blocked the penetration of ovules by supernumerary pollen tubes, we turned to the fact that pollen tubes depend on chemoattractants such as LUREs^{1,2,5,6} to guide them to ovules. To prevent the approach of late-arriving pollen tubes, the tube that arrives first at an ovule could trigger a mechanism to disengage the guidance process. Because NO is gaseous, capable of modifying target molecules²¹⁻²³ and concentrated at the filiform apparatus upon penetration by the first pollen tube (Fig. 2a-c), it could potentially target and modify the cysteine-rich LUREs^{1,2}. In examining whether NO might affect the pollen tube attraction mediated by LUREs, we observed that the arrival of pollen tubes at ovules expressing LURE1-GFP¹¹ correlated with the delocalization of the attractant from the filiform apparatus to the synergid cytoplasm (Fig. 4a, b). Moreover, treatments with S-nitrosoglutathione (GSNO) or sodium nitroprusside (SNP) (both of which generate NO) and PGA all similarly induced a retention of LURE1-GFP in the synergid cells of ovules from unpollinated pistils (Fig. 4a, Extended Data Fig. 6a-c). In vitro, GSNO induced multimers of LURE1 tagged with maltose binding protein (MBP-LURE1), inhibited binding of the attractant to its receptor PRK6^{26,27} and suppressed the activity of MBP-LURE1 to attract pollen tubes in semi-in vivo attraction assays^{1,26} (Fig. 4c, d, Extended Data Fig. 6d-k). These results imply that the NO condition at the filiform apparatus after the arrival of the first pollen tube could disengage pollen tube attraction by a two-pronged mechanism that inhibits the activity of the already secreted attractant and prevents further secretion of attractant to reform a gradient.

We further determined that NO modifies LURE1 and that these modifications affect the efficacy of the attractant. LUREs have three pairs of disulfide bonds $^{\rm L26,27}$. Nano-liquid chromatography with tandem mass spectrometry (LC–MS/MS) analysis of MBP–LURE1 nitrosated by GSNO and labelled with a tandem mass tag (TMT) showed that Cys84 of LURE1

was nitrosated (Fig. 4e–g, Extended Data Fig. 7a, b, e, Supplementary Fig. 1). A natural mutation at Cys84 renders LURE1.5 nonfunctional (Extended Data Fig. 8), providing a genetic implication for the potential importance of NO modification at Cys84 to LURE activity.

We noted that Cys17 in the LURE1 signal peptide is a predicted target for nitrosation (using GPS-SNO (www.sno.biocuckoo.org)). When expressed in Arabidopsis, LURE1(C17A)-GFP was localized inside the synergid cells even before pollination (Fig. 4i), unlike the normal location of LURE1 at the filiform apparatus (Fig. 4a, Extended Data Fig. 7f). LC-MS/MS analysis of full-length LURE1 precursor treated by GSNO and labelled by TMT showed that Cys17 was indeed nitrosated (Fig. 4e, f, h, Extended Data Fig. 7c, d). These observations provide biochemical and molecular support for how NO induced by the arrival of the first pollen tube suppresses the entrance of supernumerary pollen tubes, by modifying secreted LURE1 to inhibit its activity and intracellular LURE1 to suppress its secretion to replenish an active attractant. The fact that Cys17 and Cys84 are conserved among the broader LURE family^{1,2} (Extended Data Fig. 8) suggests that pollen tube arrival at ovules could affect the efficacy of widespread chemoattractants to prevent penetration by late-arriving pollen tubes.

Discussion

How FER mediates sperm release⁴ and prevents ovules from penetration by multiple pollen tubes (summarized in Extended Data Fig. 9) suggest an intricate multilayered strategy that flowering plants have evolved to ensure reproductive success. The molecular property of FER^{3,15} is well-suited to serve these two intimately linked but opposed processes—enabling fertilization and suppressing unwanted fertilization. The interaction between the extracellular domain of FER and pectin¹⁵ could link cell wall quality control to maintaining a source for biologically active pectic moieties, generated by processes such

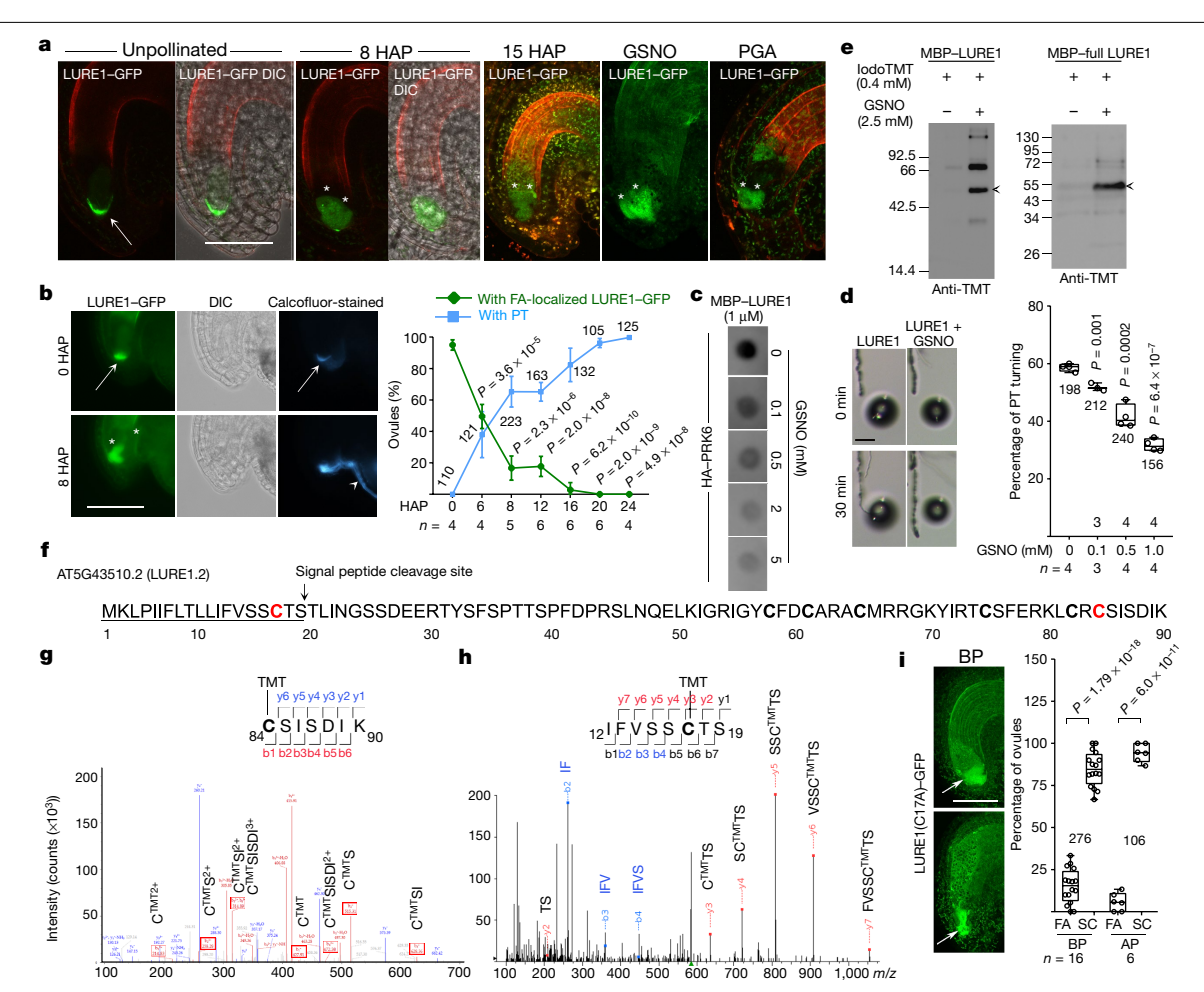


Fig. 4 | NO affects LURE1 and suppresses pollen tube attraction. a, LURE1-GFP localization. Ovules from unpollinated and pollinated pistils (8 and 15 h after pollination). GSNO- and PGA-treated ovules from unpollinated pistils were examined by confocal microscopy. Experiments were carried out four times with comparable results. **b**, LURE1-GFP localization and pollen tube penetration. Ovules expressing LURE1-GFP from pollinated pistils were observed, followed by staining with calcofluor white to reveal pollen tubes. Data shown are average \pm s.d., n = pistils. **c**, **d**, Effect of GSNO on the interaction between LURE1 and the receptor PRK6, and pollen tube attraction. c, Filterbinding assay showed dose-dependent inhibition of MBP-LURE1 binding to $hae magglutinin (HA) \text{-} tagged PRK6 \, extracellular \, domain^{26,27} \, by \, GSNO. \, \boldsymbol{d}, Pollender \, domain^{26,27} \, by \, GSNO. \, \boldsymbol{d}, Pollender \, domain^{26,27} \, by \, GSNO. \, \boldsymbol{d}, Pollender \, domain^{26,27} \, by \, GSNO. \, \boldsymbol{d}, Pollender \, domain^{26,27} \, by \, GSNO. \, \boldsymbol{d}, Pollender \, domain^{26,27} \, by \, GSNO. \, \boldsymbol{d}, Pollender \, domain^{26,27} \, by \, GSNO. \, \boldsymbol{d}, Pollender \, domain^{26,27} \, by \, GSNO. \, \boldsymbol{d}, Pollender \, domain^{26,27} \, by \, GSNO. \, \boldsymbol{d}, Pollender \, domain^{26,27} \, by \, GSNO. \, \boldsymbol{d}, Pollender \, domain^{26,27} \, by \, GSNO. \, \boldsymbol{d}, Pollender \, domain^{26,27} \, by \, GSNO. \, \boldsymbol{d}, Pollender \, domain^{26,27} \, by \, GSNO. \, \boldsymbol{d}, Pollender \, domain^{26,27} \, by \, GSNO. \, \boldsymbol{d}, Pollender \, domain^{26,27} \, by \, \boldsymbol{d}, Pollender \, \boldsymbol{d}, Pollender$ tube attraction assays^{1,37} showed GSNO inhibition of MBP-LURE1 activity. Twomicromolar MBP-LURE1 was used in the gelatin beads (dark spots). Data shown are average \pm s.d. n = 4 replicates; numbers in the plot indicate pollen tubes examined. e-h, Mass spectrometry analysis of GSNO-treated MBP-LURE1 and MBP-full-length LURE1. Nitrosated amino acid residues were labelled with TMT³⁸. e, Immunoblot of TMT-labelled proteins. f, Sequence of full-length

LURE1.2 (ref. 1); mature LURE1.2 starts at T, right after signal peptide cleavage site (indicated by arrow). Cysteines are highlighted in bold; Cys17 and Cys84 (in red) are nitrosated. g. h. LC-MS/MS spectra showed the presence of peptides labelled with TMT at Cys84 from MBP-LURE1 (g), and peptides labelled with TMT at Cys17 from MBP-full-length LURE1 (h). Nitrosated Cys84 (g) and Cys17 (h) were observed in two and three independent experiments, respectively. Proteins in e were representative of more than three independent preparations. i, Localization of LURE1p::LURE1(C17A)-GFP in ovules before pollination (BP) and after pollination (AP). Data shown are average ± s.d., n indicates the number of pistils. P values were obtained using two-tailed t-tests. Data in **b-d**, **i** are representative of three independent experiments; numbers in data plots indicate the total number of ovules (b, i) or pollen tubes (d) examined. Scale bars, 50 μm. Asterisks denote synergid cells (a, b); red, autofluorescence (a). Arrows, filiform apparatus (a, b), synergid cells (i); arrowhead, pollen tube (b), TMT-labelled target proteins (e). Box plots: centre line, median; box limits, lower and upper quartiles; dots, individual data points; whiskers, highest and lowest data points.

as fungal²⁵ and pollen tube growth. Signal-elicited cascades could be propagated by FER-regulated RHO GTPases¹⁰ to diverse responses. Such functional versatility could allow FER to sensitively link the effect of its first act in the ovular environment to elicit conditions fitting for its second act.

The use of NO as an agent to disengage pollen tube attraction could be founded on its gaseous, fast-acting ability to modify other molecules^{21,23}. Although the precise working distance for NO is not known, the FER-mediated blockade for late-arriving pollen tubes could be enacted along the gradient of attractants—and potentially even beyond this gradient, owing to the higher diffusability of NO (Extended Data Fig. 10f). The diffusability of NO is consistent with the fact that rarely more than a single pollen tube enters an ovule and that the deterrence of latecomers occurs rapidly upon arrival of the first pollen tube^{5,6}. LUREs, being cysteine-rich proteins, are also perfect targets for NO-mediated suppression of their activity when fertilization is ascertained. NO dissipation from the filiform apparatus region of a penetrated, but not fertilized, ovule could allow for a regeneration of the chemoattractant gradient. This could lead to some recovery of the ability to attract pollen tubes to potentiate fertilization recovery¹²⁻¹⁴ (Extended Data Fig. 10g-i). Pollen tube-ovule interaction occurs in highly restricted spatial and temporal windows, which renders mechanistic dissection extremely challenging. The molecular insights discussed here provide a basis for understanding

the many cell-cell communicative processes that work concertedly for reproductive success in plants.

Online content

Any methods, additional references, Nature Research reporting summaries, source data, extended data, supplementary information, acknowledgements, peer review information; details of author contributions and competing interests; and statements of data and code availability are available at https://doi.org/10.1038/s41586-020-2106-2.

- Takeuchi, H. & Higashiyama, T. A species-specific cluster of defensin-like genes encodes diffusible pollen tube attractants in Arabidopsis. PLoS Biol. 10, e1001449 (2012).
- Zhong, S. et al. Cysteine-rich peptides promote interspecific genetic isolation in Arabidopsis. Science 364, eaau9564 (2019).
- Li, C., Wu, H. M. & Cheung, A. Y. FERONIA and her pals: functions and mechanisms. Plant Physiol. 171, 2379-2392 (2016).
- Duan, Q. et al. Reactive oxygen species mediate pollen tube rupture to release sperm for fertilization in Arabidopsis. Nat. Commun. 5, 3129 (2014).
- Dresselhaus, T. & Franklin-Tong, N. Male-female crosstalk during pollen germination, tube growth and guidance, and double fertilization. Mol. Plant 6, 1018-1036 (2013).
- Higashiyama, T. & Yang, W. C. Gametophytic pollen tube guidance: attractant peptides, gametic controls, and receptors. Plant Physiol. 173, 112-121 (2017).
- Wu, H., de Graaf, B., Mariani, C. & Cheung, A. Y. Hydroxyproline-rich glycoproteins in plant reproductive tissues: structure, functions and regulation. Cell. Mol. Life Sci. 58, 1418-1429 (2001).
- Cheung, A. Y., Wang, H. & Wu, H. M. A floral transmitting tissue-specific glycoprotein attracts pollen tubes and stimulates their growth. Cell 82, 383-393 (1995).
- 9. Escobar-Restrepo, J. M. et al. The FERONIA receptor-like kinase mediates male-female interactions during pollen tube reception. Science 317, 656-660 (2007).
- Duan, Q., Kita, D., Li, C., Cheung, A. Y. & Wu, H.-M. FERONIA receptor-like kinase regulates RHO GTPase signaling of root hair development. Proc. Natl Acad. Sci. USA 107, 17821-17826 (2010).
- Punwani, J. A., Rabiger, D. S. & Drews, G. N. MYB98 positively regulates a battery of synergid-expressed genes encoding filiform apparatus localized proteins. Plant Cell 19, 2557-2568 (2007)
- Beale, K. M., Leydon, A. R. & Johnson, M. A. Gamete fusion is required to block multiple pollen tubes from entering an Arabidopsis ovule. Curr. Biol. 22, 1090-1094 (2012).
- Kasahara, R. D. et al. Fertilization recovery after defective sperm cell release in Arabidopsis. Curr. Biol. 22, 1084-1089 (2012).
- 14. Maruyama, D. et al. Rapid elimination of the persistent synergid through a cell fusion mechanism. Cell 161, 907-918 (2015).
- Feng, W. et al. The FERONIA receptor kinase maintains cell-wall integrity during salt stress through Ca2+ signaling. Curr. Biol. 28, 666-675.e5 (2018).
- Peaucelle, A., Braybrook, S. & Höfte, H. Cell wall mechanics and growth control in plants: the role of pectins revisited. Front. Plant Sci. 3, 121 (2012).
- Hou, W.-C., Chang, W.-H. & Jiang, C.-M. Qualitative distinction of carboxyl group distribution in pectins with ruthenium red. Bot. Bull. Acad. Sin. 40, 115-119 (1999).

- Pattathil, S. et al. A comprehensive toolkit of plant cell wall glycan-directed monoclonal antibodies. Plant Physiol. 153, 514-525 (2010).
- Peaucelle, A. et al. Arabidopsis phyllotaxis is controlled by the methyl-esterification status of cell-wall pectins. Curr. Biol. 18, 1943-1948 (2008).
- Wolf, S., Mravec, J., Greiner, S., Mouille, G. & Höfte, H. Plant cell wall homeostasis is mediated by brassinosteroid feedback signaling. Curr. Biol. 22, 1732-1737 (2012).
- Besson-Bard, A., Pugin, A. & Wendehenne, D. New insights into nitric oxide signaling in plants. Annu. Rev. Plant Biol. 59, 21-39 (2008).
- Domingos, P., Prado, A. M., Wong, A., Gehring, C. & Feijo, J. A. Nitric oxide: a multitasked signaling gas in plants. Mol. Plant 8, 506-520 (2015).
- Planchet, E. & Kaiser, W. M. Nitric oxide (NO) detection by DAF fluorescence and chemiluminescence: a comparison using abiotic and biotic NO sources. J. Exp. Bot. 57, 3043-3055 (2006).
- Boavida, L. C., Borges, F., Becker, J. D. & Feijó, J. A. Whole genome analysis of gene expression reveals coordinated activation of signaling and metabolic pathways during pollen-pistil interactions in Arabidopsis. Plant Physiol. 155, 2066-2080 (2011).
- 25. Rasul, S. et al. Nitric oxide production mediates oligogalacturonide-triggered immunity and resistance to Botrytis cinerea in Arabidopsis thaliana, Plant Cell Environ, 35, 1483-1499 (2012).
- Takeuchi, H. & Higashiyama, T. Tip-localized receptors control pollen tube growth and LURE sensing in Arabidopsis. Nature 531, 245-248 (2016).
- Zhang, X. et al. Structural basis for receptor recognition of pollen tube attraction peptides. Nat. Commun. 8, 1331 (2017).
- Clausen, M. H., Willats, W. G. & Knox, J. P. Synthetic methyl hexagalacturonate hapten inhibitors of anti-homogalacturonan monoclonal antibodies LM7, JIM5 and JIM7. Carbohydr. Res. 338, 1797-1800 (2003).
- Hruz, T. et al. Genevestigator v3: a reference expression database for the meta-analysis of transcriptomes. Adv. Bioinformatics 2008, 420747 (2008).
- Huang, Y. C. et al. PECTIN METHYLESTERASE34 contributes to heat tolerance through its role in promoting stomatal movement. Plant Physiol. 174, 748-763 (2017).
- Terrile, M. C. et al. Nitric oxide influences auxin signaling through S-nitrosylation of the
- Arabidopsis TRANSPORT INHIBITOR RESPONSE 1 auxin receptor. Plant J. 70, 492-500 (2012). 32. Prado, A. M., Porterfield, D. M. & Feijó, J. A. Nitric oxide is involved in growth regulation
- and re-orientation of pollen tubes. Development 131, 2707-2714 (2004). Wilkinson, J. Q. & Crawford, N. M. Identification and characterization of a chlorateresistant mutant of Arabidopsis thaliana with mutations in both nitrate reductase structural genes NIA1 and NIA2. Mol. Gen. Genet. 239, 289-297 (1993).
- Sanz, L. et al. Nitric oxide plays a role in stem cell niche homeostasis through its interaction with auxin. Plant Physiol. 166, 1972-1984 (2014).
- Guo, F. Q., Okamoto, M. & Crawford, N. M. Identification of a plant nitric oxide synthase gene involved in hormonal signaling. Science 302, 100-103 (2003).
- Moreau, M., Lee, G. I., Wang, Y., Crane, B. R. & Klessig, D. F. AtNOS/AtNOA1 is a functional Arabidopsis thaliana cGTPase and not a nitric-oxide synthase. J. Biol. Chem. 283, 32957-32967 (2008)
- Okuda, S. et al. Defensin-like polypeptide LUREs are pollen tube attractants secreted from synergid cells. Nature 458, 357-361 (2009).
- Qu, Z. et al. Proteomic quantification and site-mapping of S-nitrosylated proteins using isobaric iodoTMT reagents. J. Proteome Res. 13, 3200-3211 (2014).

Publisher's note Springer Nature remains neutral with regard to jurisdictional claims in published maps and institutional affiliations

© The Author(s), under exclusive licence to Springer Nature Limited 2020

Methods

Plant material, growth, transformation and pollination

Arabidopsis thaliana Col-O plants were maintained at 22 °C in growth chambers. fer-4 (GK-106A06, GABI-Kat) transformed Arabidopsis and transformed Arabidopsis with FER promoter (FERp::FER-GFP) have previously been described 10. fer-4 and several other fer alleles behaved identically; fer-4 was complemented by FERp::FER-GFP^{4,10}. PME34 and PME44 are more notably expressed in ovules than are other members of the gene family²⁹. pme34 (SALK_039555C)³⁰, pme44 (SALK_071362C), nia1 nia2 (CS2356)^{33,34} and noa1(CS6511)^{35,36} were from Arabidopsis Biological Resource Center. A second pme34 (SALK 062058C) and pme44 (SALK 050157C) behaved similarly to SALK 039555C and SALK 071362C. A double pme34 pme44 line was generated by crossing pme34 (SALK 039555C) and pme44 (SALK 071362C). Seeds from LAT52::tdTomato transformed *Arabidopsis* and *hap2/*+¹² were gifts from B. McClure and M. Johnson, respectively. LURE1-GFP-expressing plants were the original DD2 promoter DD2p::DD2-GFP transformed Arabidopsis¹¹, a gift from G. Drews; DD2 is equivalent to LURE1 (At5g43510)¹. LURE1p::LURE1-(C17A)-GFP and FERp::PMEI1 (pectin methylesterase inhibitor 1; At 1g48020)-GFP were transformed into wild-type A. thaliana (Col-0) by floral dip³⁹. PMEIox (35S:PMEI5) seeds²⁰ were a gift from H. Hofte. *aca9-1* seeds⁴⁰ were a gift from J. Harper. Hand pollination experiments were carried out using wild-type pollen as the male donor unless otherwise noted, and wild type or fer-4 as the female parents as indicated in the text or figure legends.

Microscopy

Epifluorescence and DIC microscopy were carried out on a NIKON Eclipse E800 microscope equipped with a SPOT charge-coupled device (Molecular Diagnostic). Filters Ex460-500/DM505/BA510-560 (FITC, green), Ex546(10)/DM565LP/EM590LP (rhodamine, red), and Ex330-380/DM400/BA420 (blue) from Chroma were used. Confocal microscopy was carried out on a Nikon A1. Unless otherwise indicated in figure legends, quantitative data are from one representative of at least three independent experiments; most assays were repeated at least five times. For every experiment, each dataset was obtained from ovules isolated from 6-9 pistils, each yielding about 20-30 goodquality ovules. Data (per cent of ovules with multiple pollen tubes, or filiform apparatus with de-esterified pectin, NO or LURE1-GFP) from each pistil were averaged and represented in data bars/points. Error bars represent s.d. from the average, unless otherwise indicated. The n values of each data plot reflect pistils as indicated in figure legends; the numbers of ovules examined are indicated on the data plots. Student's t-tests were used for P value calculations (two-tailed). P < 0.05 and *P* < 0.01 are considered significant and highly significant differences, respectively; in most experiments, P values ranged from $P < 10^{-2}$ to $P < 10^{-5}$.

Pollen tube visualization

Pollen tube visualization was predominantly carried out by aniline blue $(0.1\%)^2$ to stain callose in the pollen tube cell wall. Cessation of the fluorescent signal at the entrance to the female gametophyte reflected pollen tube rupture and sperm release upon penetrating a synergid cell. The pile-up of aniline-blue-stained material inside the *fer* female gametophyte reflected a failure of pollen tube rupture^{4,9}. Multiple or supernumerary pollen tube entrance refers to two or more pollen tubes entering the micropyle of a single ovule. Often multiple pollen tubes appeared as a thicker bundle outside the targeted *fer-4* ovule relative to the single pollen tube that targeted a wild-type ovule under normal conditions. In experiments in which aniline blue was not used, calcofluor white (0.01%) (a cellulose stain 41,42) was used to mark the pollen tube outside of a penetrated ovule. LAT52::tdTomato-expressing pollen tubes were used to mark the synergid cell of a penetrated ovule as cytoplasmic discharge from an entered pollen tube would render it

red-fluorescent, allowing the synergid cell and filiform apparatus be clearly defined.

Detection of ovule pectin, NO and LURE1-GFP signals

Ovules were isolated from pistils and transferred to $40\,\mu l$ of corresponding solution for treatment for individual purposes. The procedures were all carried out on a microscope slide under a cover glass at room temperature in a box humidified with several layers of moist paper towel. Buffer exchanges between steps were carried out five times by depletion of used buffer from one side using a filter-paper wedge and application of new buffer from the other side.

Ovule pectin detection was carried out by ruthenium red (RuR)¹⁷ (PolySciences), and the monoclonal antibodies JIM5, JIM7 and M38 18,28 (gifts from I.P. Knox and later purchased from Complex Carbohydrate Research Center). Though not specific for pectin, RuR is commonly used as a histochemical stain for pectin (for example, in pollen tubes⁴³) and had previously been used to approximate de-esterified pectin⁴³⁻⁴⁵. JIM5 and JIM7, respectively, detect partially methylesterified homogalacturonan epitope (about 40% unesterified residues adjacent to, or flanked by, residues with methylester groups) and partially methylesterified homogalacturonan epitope (methylesterified residues up to 80%)²⁸. M38 detects fully de-esterified homogalacturonan¹⁸. Ovules from naturally pollinated or hand-pollinated pistils were used as indicated in the text. For hand pollination, stage 12c (approaching the end of the context of theof stage 12) flower buds^{4,46} were emasculated and allowed to mature for 24 h (reaching early to mid-stage 14). They were either pollinated or left unpollinated. Individual ovules were isolated from the pistils at 20 h after pollination or as otherwise indicated. For RuR histochemical staining, dissected ovules were immersed in RuR (0.05% in H₂O) for 3-4 min and washed with H₂O before observation under DIC. For immunodetection, ovules were immediately transferred to fixative (4% paraformaldehyde in phosphate buffered saline (PBS), 20 mM Naphosphate, pH7.4, 100 mM NaCl) for 1 h and then processed for pectin detection. The ovules were first rinsed in PBS, then blocked in 3% nonfat milk (Stop & Shop) in PBS for 1 h, incubated with JIM5 (1:500), M38 (1:50) or JIM7 (1:50) for 2 h, washed with PBS, then incubated with FITClabelled secondary antibody against mouse or rat antibodies (1:100, Santa Cruz) for 2 h, washed and imaged by wide-field epifluorescence (Nikon Eclipse E800) using the FITC filter.

For NO detection, DAF-DA (Cayman Chemical, cat no. 85165) was used³¹. Chemicals used to generate or scavenge NO included: GSNO (Sigma-Aldrich) and SNP (Alfa Aesar) generate NO; cPTIO (2-(4-carboxyphenyl)-4,5-dihydro-4,4,5,5-tetramethyl-1*H*-imidazolyl-1-oxy-3-oxide, monopotassium salt) (Cayman Chemical) scavenges $NO^{22,31,32}$. For chemical treatments, stock solutions were prepared in DMSO and diluted to working concentrations in 20 mM HEPES (pH7.5) with 100 µM DAF-DA. Mock treatments had identical final DMSO concentration as in experimental conditions. PGA (Sigma) was fragmented by sonication before use15; the sample was assessed by polyacrylamide gel electrophoresis followed by RuR (0.02%) staining⁴⁷. Ovules from unpollinated or pollinated wild-type pistils were used as indicated in the text using wild-type pollen or tdTomato-expressing pollen. Individual ovules were isolated from the pistils at the specified number of hours after pollination, and immediately transferred to 100 µM DAF-DA (20 mM HEPES, pH 7.5) on a slide, incubated under a coverslip for 1 h in a humidified box in the dark. They were then washed in the buffer and observed immediately by epifluorescence using the FITC filter cube.

For the effect of PGA on ovule NO, 4 μ l of PGA (final concentrations indicated in figures or figure legends) were added to DAF-DA solution (total 40 μ l treatment volume) for NO detection. For pollination-affected ovule NO, wild-type, fer-4, nia1 nia2 and noa1 pistils were pollinated with wild-type pollen or tdTomato-expressing pollen, and ovules were processed for NO detection at 16–20 h after pollination as described unless otherwise indicated. tdTomato-labelled pollen tubes ejected red cytoplasm inside the synergid cell, providing a spatial

reference for the synergid cells and easier definition for the filiform apparatus. When wild-type pollen was used, calcofluor white was used to visualize pollen tube entry; the cell-wall stain was added and imaged after the NO signal was acquired.

For microscopic localization of LURE1–GFP and LURE1(C17A)–GFP, ovules isolated from unpollinated or pollinated pistils, or ovules from unpollinated pistils either mock- or chemically (GSNO and SNP) treated were used as indicated in the text and figure legends.

For data quantification, samples were observed by epifluorescence and signals were assessed by two methods. First (and similar to methods previously described for the reactive oxygen species signal of the filiform apparatus region⁴), images acquired under identical conditions for comparative samples were analysed by Imagel. Total signal intensity from an identical area covering the filiform apparatus region from each ovule was quantified by ImageJ. The signal intensity from an identical area in the synergid cell was measured similarly for background. The ovule was scored as NO- or de-esterified-pectin-positive, if the ratio of the filiform apparatus to synergid cell was greater than 1.2. An alternate and more expeditious method was based on the evaluation of signal intensity in the filiform apparatus and synergid cell by direct scoring during observation. Ovules with obvious signal in the filiform apparatus were scored as positive. For each set of studies, a comparative assessment between the two methods was first made; both methods consistently yielded similar outcomes. Direct counting of ovules with obvious NO signals minimized exposure time and allowed expeditious scoring of a large number of ovules. Camera acquisition of images followed by ImageJ analyses was applied for at least one set of ovules and also from time to time within an experiment for data conformation. Comparison of the two assessment methods is provided in Extended Data Figs. 3, 5.

Seedling NO studies

Arabidopsis seeds were surface-sterilized and germinated on B5 medium with 0% sucrose and solidified by 0.7% agar. Seeds were cold-treated at 4 °C for 2 d to synchronize germination, then transferred to room temperature. Plates were left standing vertically for seedling growth under 16/8 h light/dark cycles. Three-day-old seedlings were submerged in 5 μ M DAF-DA in 20 mM HEPES (pH 7.5), either unsupplemented or supplemented with increasing concentrations of sonicated PGA fragments for 3.5 h in the dark. The seedlings were washed in 20 mM HEPES (pH 7.5), and transferred to glass slides in the same buffer for fluorescence and DIC microscopy. At least ten seedlings were examined for each condition; data are presented as average \pm s.d. from one representative of at least three independent replicates for each condition. Fluorescent images were acquired under identical conditions for comparative studies and signal intensity was quantified through Image], as described previously for fluorescent signal in seedling roots 4 .

Preparation of pistil exudate and analysis

Exudates from unpollinated and pollinated pistils were prepared. Stage 12c flower buds from wild-type or fer-4 plants were emasculated, left unpollinated or hand-pollinated by wild-type pollen. Pistillate exudate preparation followed a previously published method⁴⁸, with modifications. At 14 hafter pollination, both pollinated and unpollinated pistils (100 per preparation) were placed horizontally on the double-sided tape. The transmitting tissue from 20 pistils and attached ovules were scraped and transferred to 500 µl of H₂O in a microfuge tube. The tubes were incubated at 60 °C for 6 h, then 40 °C with the cap open overnight to allow evaporation of excess H₂O. The crude exudate (from 100 pistils) was then pooled, dried in a speed-vacuum and resuspended in 20 μl of H₂O. De-esterified pectin contents in these exudates were approximated by spotting 2-4 μl of exudates and a concentration series of fragmented PGA quantified according to a previous study⁴⁷ on nylon filter membranes, followed by immunoblot detection using JIM5 antibodies and chemiluminescence after secondary antibody binding. For pectin quantification before use in biological assays, 2 µl of each

pistillate exudate sample was spotted on a nylon filter membrane, airdried for 30 min, followed by immunodetection of de-esterified pectin using JIM5 or M38 antibodies. An identical membrane was stained by toluidine blue (0.005%) for 5 min to ascertain comparable applications of pistillate exudates. For ovule treatment, 4 μl (of 20 μl preparations from 100 pistils; that is, equivalent to 20 pistils) of exudate were used for each ovule treatment, followed by NO detection as described in 'Detection of ovule pectin, NO and LURE1–GFP signals'.

Purification of LURE1 and LURE1 receptor PRK6

LURE1 ((LURE1.2 (At5g43510))¹ and its receptor PRK6 (At5g20690)²⁶ from Arabidopsis were used. To obtain purified proteins, MBP-LURE1 (amino acid residues 20-90) and His,-HA-PRK6 extracellular domain (HA-PRK6(ecd)) (residues 1-262²⁷) were cloned in pMAL (NEBL) and pET21 (Invitrogen), respectively, for expression in Escherichia coli BL21. MBP-LURE1 production was induced by IPTG (0.5 mM) during growth at either 37 °C for 6 h or 16 °C overnight. Cells were resuspended in lysis buffer (40 mM Tris-Cl pH 7.5, 150 mM NaCl, 1 mM EDTA, using 15 ml per pellet from 800-ml cultures), flash-frozen, thawed and sonicated 5 times, 10-s each. After clearing the debris by centrifugation, the lysate was loaded onto an amylose column pre-equilibrated with lysis buffer. The resin was extensively washed in the same buffer, and bound proteins were eluted by 10 mM maltose in lysis buffer. Tubes with peak protein concentrations were pooled and dialysed into TBS (25 mM Tris-Cl pH 7.5, 100 mM NaCl) overnight, at 4 °C. If concentration was needed, the protein was passed through a centricon with a 10-kDa molecular mass cut off).

HA–PRK6(ecd) was expressed in $\it E. coli$ at 37 °C. Fifteen millilitres of urea lysis buffer (8 M urea 50 mM Tris-Cl pH 7.5, 300 mM NaCl) was used per 800-ml culture and the cell suspension was sonicated once for 10 s. The lysate was applied to a urea lysis buffer-equilibrated Talon (Clontech) column (1 ml), washed with 5 ml urea lysis buffer and bound proteins were eluted with 5 ml of 250 mM imidazole in urea lysis buffer and collected in 1-ml fractions. The elution was then dialysed overnight into TBS.

Quality of the purified proteins was assessed by SDS-PAGE (15%) followed by Coomassie-blue staining and immunoblot detection using antibody against the respective tag.

Protein binding assays for LURE1-receptor interaction

A filter binding assay¹⁵ was used. Equal volumes (1.5 µl) of a serial dilution of purified HA-PRK6(ecd) was spotted on nitrocellulose membrane (Bio-Rad) and air-dried for 15 min. stained in Ponceau S (3% acetic acid. 0.2% Ponceau S) for 5 min to reveal protein dots to ascertain quality and comparable protein application. After Ponceau S removal, the membrane was blocked twice, 30 min each, in TBST (25 mM Tris-Cl pH 7.5, 100 mM NaCl, 0.1% Tween-20) and 3% dried milk. It was rinsed once with TBS (25 mM Tris-Cl pH 7.5, 100 mM NaCl) for 3 min, then incubated with 1 μM MBP-LURE1 in TBS at room temperature with gentle shaking for 1h. The membrane was washed 5 times, 3 min each, with TBST. Immunodetection of bound MBP-LURE1 was carried out by incubation with anti-MBP antibody (NEBL, 1:2,000 dilution) in TBST and 3% dried milk for 1h. The membrane was washed 5 times, 3 min each, with TBST then incubated with HRP-conjugated secondary antibody (Santa Cruz, 1:2,000 dilution) in TBST with 3% dried milk for 1h. The membrane was washed 5 times, 3 min each in TBST, and once in TBS for 3 min and developed for 3 min in reagents for chemiluminescence detection (PXi, Syngene).

Pollen tube attraction assays

MBP-LURE1 and MBP control were used under semi-in vivo pollen tube growth conditions as previously described $^{1.37}$. In brief, 2 μ l of purified MBP-LURE1 with or without GSNO treatment were mixed with 2 μ l of 10% (w/v) gelatin (Bio-Rad) pre-melted at 40 °C. After adding 150 μ l of hydrated silicone oil, they were mixed by vortexing and immediately cooled on ice to allow the formation of gelatin beads. Single beads (about 40 μ m in diameter) were picked up by a glass needle and placed at an angle of about 45–90° and slightly ahead (\leq 50 μ m) of an elongating pollen tube.

The pollen tubes that made a change in growth trajectory >20° towards the beads were scored as a positive response, as previously described³⁷.

Electrophoretic analysis of LURE1 nitrosation

GSNO was used as NO donor. MBP, MBP-LURE1 and MBP-full-length LURE1 (residues 1–90) were incubated with GSNO for 30 min at room temperature and in the dark. SDS-PAGE (5×) loading dye (without β -mercaptoethanol) was added to a final concentration of 1× loading dye (10% glycerol, 60 mM Tris-HCl, pH 6.8, 2% SDS, 0.01% bromophenol blue, no β -mercaptoethanol). Then the samples were boiled for 5 min, added to a 15% gel and run at 80 V. Gel was either stained by Coomassie blue or transferred to PVDF membrane (Perkin Elmer) for immunodetection of MBP-LURE1. When used in LURE1-HA-PRK6(ecd) interaction, MBP-LURE1 was preincubated with a concentration series of GSNO for 45 min in the dark before binding to HA-PRK6(ecd) on dot blots prepared as described in 'Protein binding assays for LURE1-receptor interaction', without or in the presence of dithiothreitol (DTT) as indicated in figures.

Mass spectrometry analysis of LURE1 nitrosation state

Preparation of in vitro nitrosated LURE1 and subsequent mass spectrometry analysis used $\it E. coli$ produced MBP-LURE1 and MBP-full-length LURE1 followed the scheme outlined in Supplementary Fig. 1. The procedure to tag nitrosated target residues for mass spectrometry analysis generally followed that provided by the user manuals of Pierce S-Nitrosylation Western Blot Kit with modification (cat. no. 90105) for protein blot detection of nitrosation and iodoacetyl tandem mass tag (iodoTMTzero) label reagent (ThermoFisher cat. no. 90100) to 'switch' nitrosated Cys residues by TMT for mass spectrometry analysis.

For TMT-labelled MBP-LURE1 and control unlabelled counterpart. proteins (Fig. 4e, Extended Data Fig. 7b) were trypsinized and analysed by nano-LC-MS/MS using an Easy-nLC 1000 nano-liquid chromatography system coupled to an Orbitrap Fusion (Thermo Scientific) tribrid mass spectrometer at the University of Massachusetts Mass Spectrometry Center. One microlitre of the trypsinized sample was injected on to a C18 trap column (75 μm × 20 mm), desalted with 5 μl of buffer A (0.1% formic acid in water), then transferred to a PepMap RSLC analytical column (75 µm × 150 mm) and eluted over a 120-min gradient from 5–40% buffer B (0.1% formic acid in acetonitrile) at 300 nl/min. MS1 data were acquired in the orbitrap at 120,000 resolution with datadependent MS/MS spectra measured in the linear ion trap using collisionally induced dissociation with 35% normalized collision energy. Raw data were processed using Proteome Discoverer 2.3, allowing for variable modifications on Cys residues by NEM, carbamidomethyl or TMTzero. Quantitation was performed by integrating the area of the parent ion peak (10 ppm mass tolerance).

Mass spectrometry analysis of TMT-labelled MBP-full-length LURE1 was carried out at the Harvard Medical School Taplin Biological Mass Spectrometry Facility. Protein bands (Fig. 4e, Extended Data Fig. 7c, d) were excised from SDS-polyacrylamide gels and processed for chymotrypsin digestion (Pierce Chymotrypsin, no. 90056). Mass spectrometry and data analysis were comparably carried out as described for MBP-LURE1.

Reporting summary

Further information on research design is available in the Nature Research Reporting Summary linked to this paper.

Data availability

Source Data for Figs. 1–4 and Extended Data Figs. 1–3, 5–7 are provided with the paper. All other data are available from the corresponding author upon request.

- Clough, S. J. & Bent, A. F. Floral dip: a simplified method for Agrobacterium-mediated transformation of Arabidopsis thaliana. Plant J. 16, 735–743 (1998).
- Schiøtt, M. et al. A plant plasma membrane Ca²⁺ pump is required for normal pollen tube growth and fertilization. Proc. Natl Acad. Sci. USA 101, 9502–9507 (2004).
- Sheng, X. et al. Lead stress disrupts the cytoskeleton organization and cell wall
 construction during *Picea wilsonii* pollen germination and tube growth. *Biol. Trace Elem.*Res. 146, 86–93 (2012).
- Chebli, Y., Kaneda, M., Zerzour, R. & Geitmann, A. The cell wall of the *Arabidopsis* pollen tube—spatial distribution, recycling, and network formation of polysaccharides. *Plant Physiol.* 160, 1940–1955 (2012).
- Leroux, C. et al. PECTIN METHYLESTERASE48 is involved in Arabidopsis pollen grain germination. Plant Physiol. 167, 367–380 (2015).
- Ischebeck, T., Stenzel, I. & Heilmann, I. Type B phosphatidylinositol-4-phosphate
 Ischiases mediate Arabidopsis and Nicotiana tabacum pollen tube growth by regulating apical pectin secretion. Plant Cell 20, 3312–3330 (2008).
- 45. Pleskot, R. et al. Turnover of phosphatidic acid through distinct signaling pathways affects multiple aspects of pollen tube growth in tobacco. Front Plant Sci. 3, 54 (2012).
- Smyth, D. R., Bowman, J. L. & Meyerowitz, E. M. Early flower development in Arabidopsis. Plant Cell 2, 755–767 (1990).
- Chormova, D., Messenger, D. J. & Fry, S. C. Boron bridging of rhamnogalacturonan-II, monitored by gel electrophoresis, occurs during polysaccharide synthesis and secretion but not post-secretion. *Plant J.* 77, 534–546 (2014).
- Nilesh, R. et al. Extraction of pectin from citrus fruit peel and use as natural binder in paracetamol tablet. Pharm. Lett. 4, 558–564 (2012).

Acknowledgements We thank G. Drews for DD2p::DD2 (AtLURE1)-GFP seeds; M. Johnson for hap2/+ seeds; B. McClure for LAT52::tdTomato transformed Arabidopsis seeds; H. Hofte for 35S:PMEI5 seeds; a large number of undergraduates who helped with plant growth and maintenance over many years, and K. McNamara and T. Lichoulas, in particular, for contributing to protein purifications: P. Huesgen and R. Tomaino for advice, and the Harvard Medical School Talpin mass spectrometry facility for service; and Y.-j. Zou for the blue-dot assay shown in Extended Data Fig. 1a. M.-C. J.L. was partially supported by the Ministry of Science and Technology Overseas Project, 2013 Graduate Student Study Abroad Program; and L.E.G.V. was partially supported by a fellowship from Estancias Posdoctorales en el Extranjero, Vinculadas a la Consolidación de Grupos de Investigación y Fortalecimiento del Posgrado Nacional 2018. This work was supported by grants from the NSF (IOS-1147165, -1146941, -1645854 and MCB-1715764 to A.Y.C. and H.-M.W.). Mass spectrometry data were partially obtained at the University of Massachusetts Mass Spectrometry Center, a facility supported by the National Institutes of Health (S100D010645); the plant growth facility was partially supported by NIFA/USDA, the Center for Agriculture, Food and the Environment, under project number MASO0525. The content is solely the responsibility of the authors and does not necessarily represent the official views of the National Institutes of Health, USDA or NIFA. Confocal microscopy was performed in the Light Microscopy Facility and Nikon Center of Excellence at the Institute for Applied Life Sciences, University of Massachusetts with support from the Massachusetts Life Science Center.

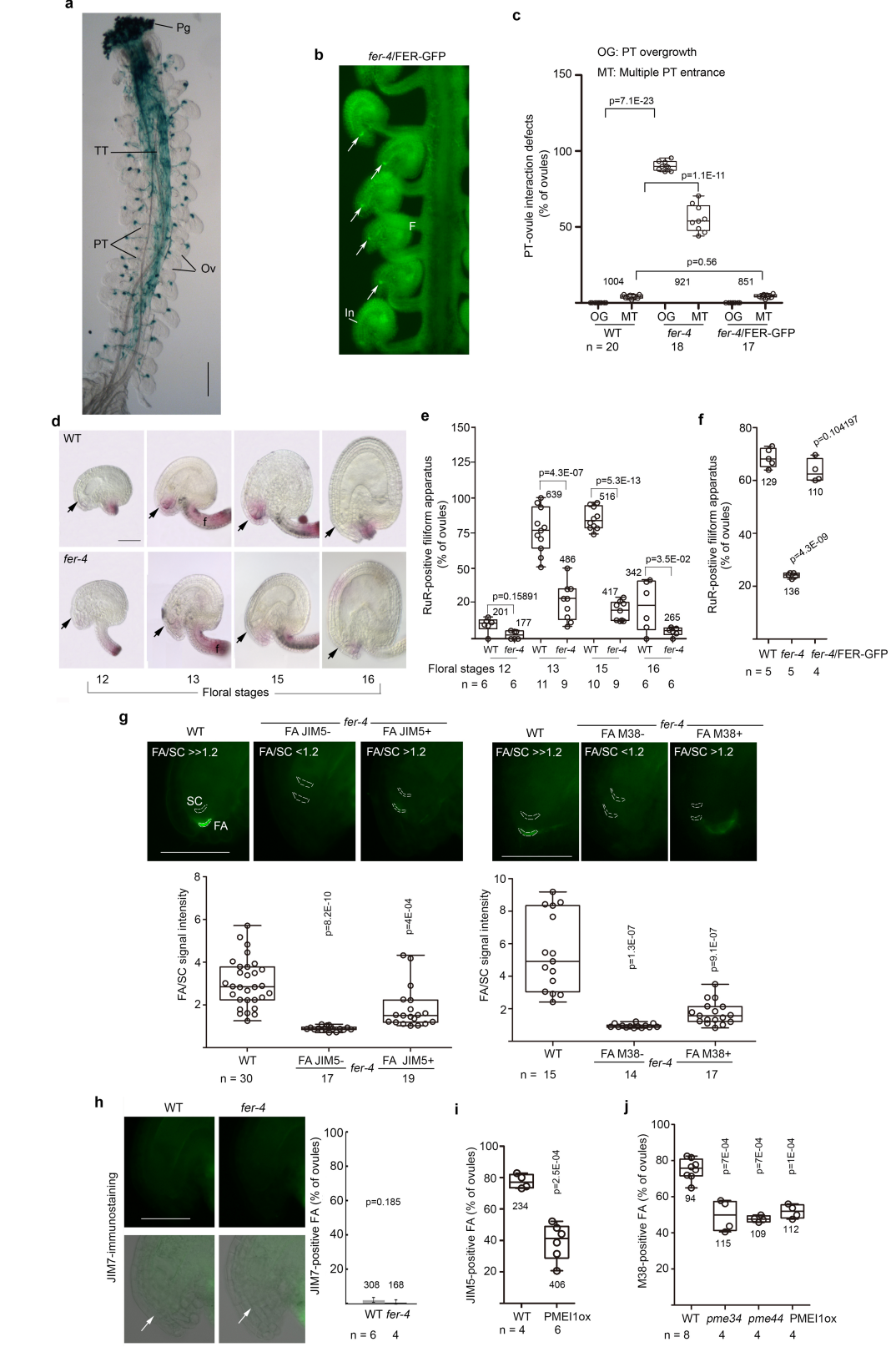
Author contributions A.Y.C. and H.-M.W. designed the overall research plan and led the writing process; Q.D. and M.-C.J.L. participated in strategy and method development for their respective focus parts, and in the writing process. Q.D. performed pollen tube-ovule interaction experiments throughout the study, with contributions to the pectin aspect from D.K. until 2012. M.-C.J.L. contributed to pectin studies and performed the biochemical studies in NO-LURE interaction (since 2013); C.S.-W. contributed to co-supervising M.-C.J.L. as a PhD mentor during the early parts of this study (2013–2015). S.J.E. provided mass spectrometry service and contributed to mass spectrometry data analysis; S.S.J., F.-L.J.Y., R.Y., H.C. and L.E.G.-V. contributed to the FER-pectin-NO-LURE biochemical studies; A.N.F., H.C. and Q.D. carried out seedling studies. All authors participated in finalizing the manuscript.

Competing interests The authors declare no competing interests.

Additional information

Supplementary information is available for this paper at https://doi.org/10.1038/s41586-020-2106-2

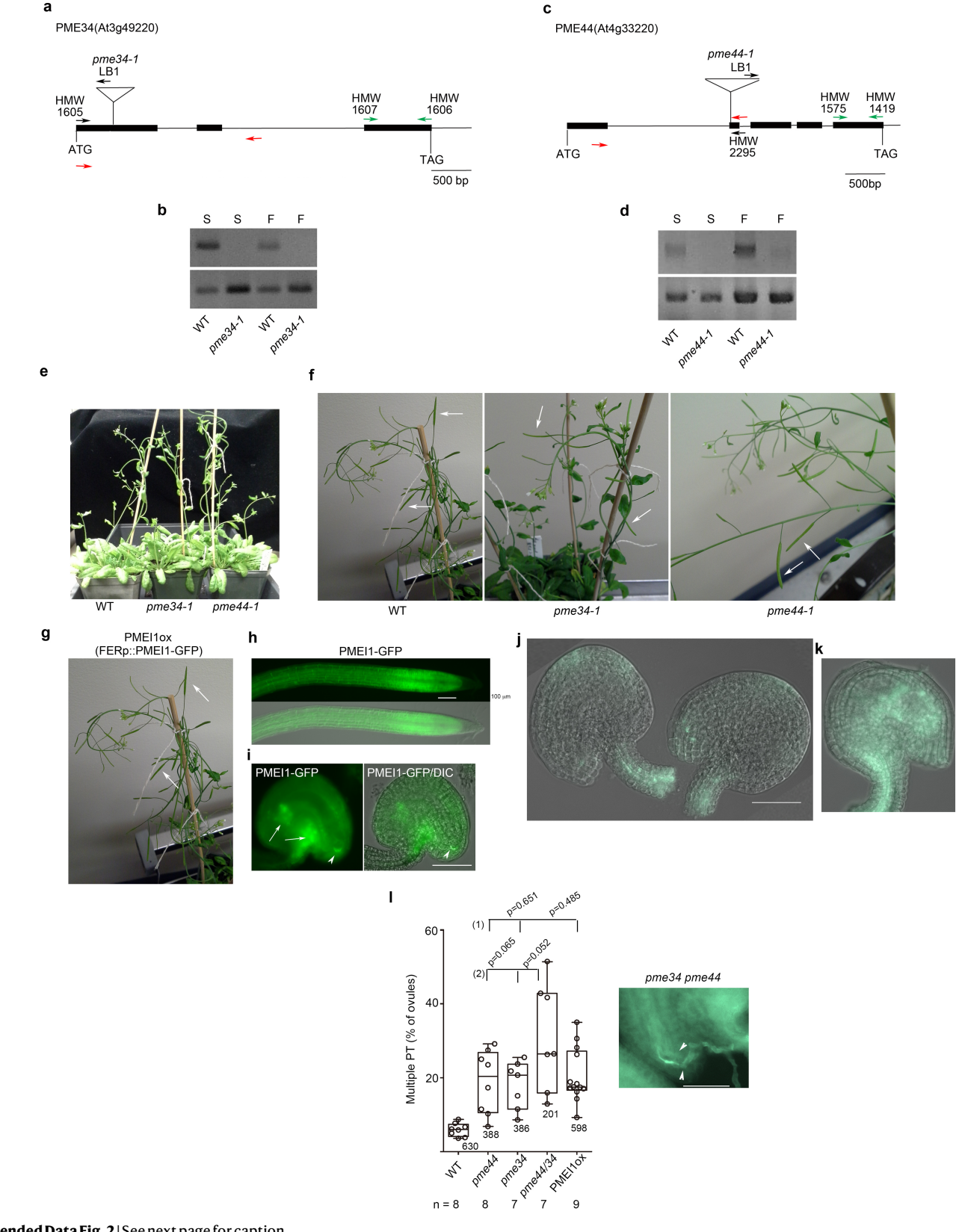
Correspondence and requests for materials should be addressed to H.-M.W. or A.Y.C. Peer review information Nature thanks John Hancock, Hermanus Hofte and the other, anonymous, reviewer(s) for their contribution to the peer review of this work. Reprints and permissions information is available at http://www.nature.com/reprints.



 $\textbf{Extended Data Fig. 1} | See \ next \ page \ for \ caption.$

Extended Data Fig. 1 | FER-regulated pollen tube-ovule interaction and pectin deposition in the filiform apparatus. a, Blue-dot assay, an alternate method (from that in Fig. 1b) to show pollen tube targeting and penetration of ovules. β-GUS-expressing pollen grains (Pg, blue) were used to pollinate a wildtype pistil, allowing the pollen tube growth path to be visualized and demonstrated the prevalently 1:1 pollen tube: ovule ratio under normal pollination conditions. This result is typical of pollinated wild-type pistils, and it was repeated at least five times in the course of this study. **b**, FER promoter (FERp)::FER-GFP expression in a complemented fer-4 pistil, showing prominent localization of FER-GFP at the filiform apparatus region (arrows)⁴ as well as expression in sporophytic tissues, such as the integuments (In) and funiculus (F). For this study, the observation was repeated at least three times in independent preparations. c, Pollen tube reception defects induced by fer-4 mutation (pollen tube overgrowth inside the female gametophyte owing to non-rupture) and multiple pollen tube entrance phenotypes. d-f, RuRdetected pectin in ovules. d, Wild-type and fer-4 ovules showed developmental regulation and FER-dependent pectin deposition at the filiform apparatus or micropylar region (arrowheads). Floral stages followed that of previous publications^{4,46}; stages 13–15 are the most receptive for pollination—at stage 16 ovules had enlarged, reflecting successful fertilization. e, Quantification of RuR-positive filiform apparatus region. f, FERp::FER-GFP complemented fer-4 mutation restored deposition of de-esterified pectin at the filiform apparatus,

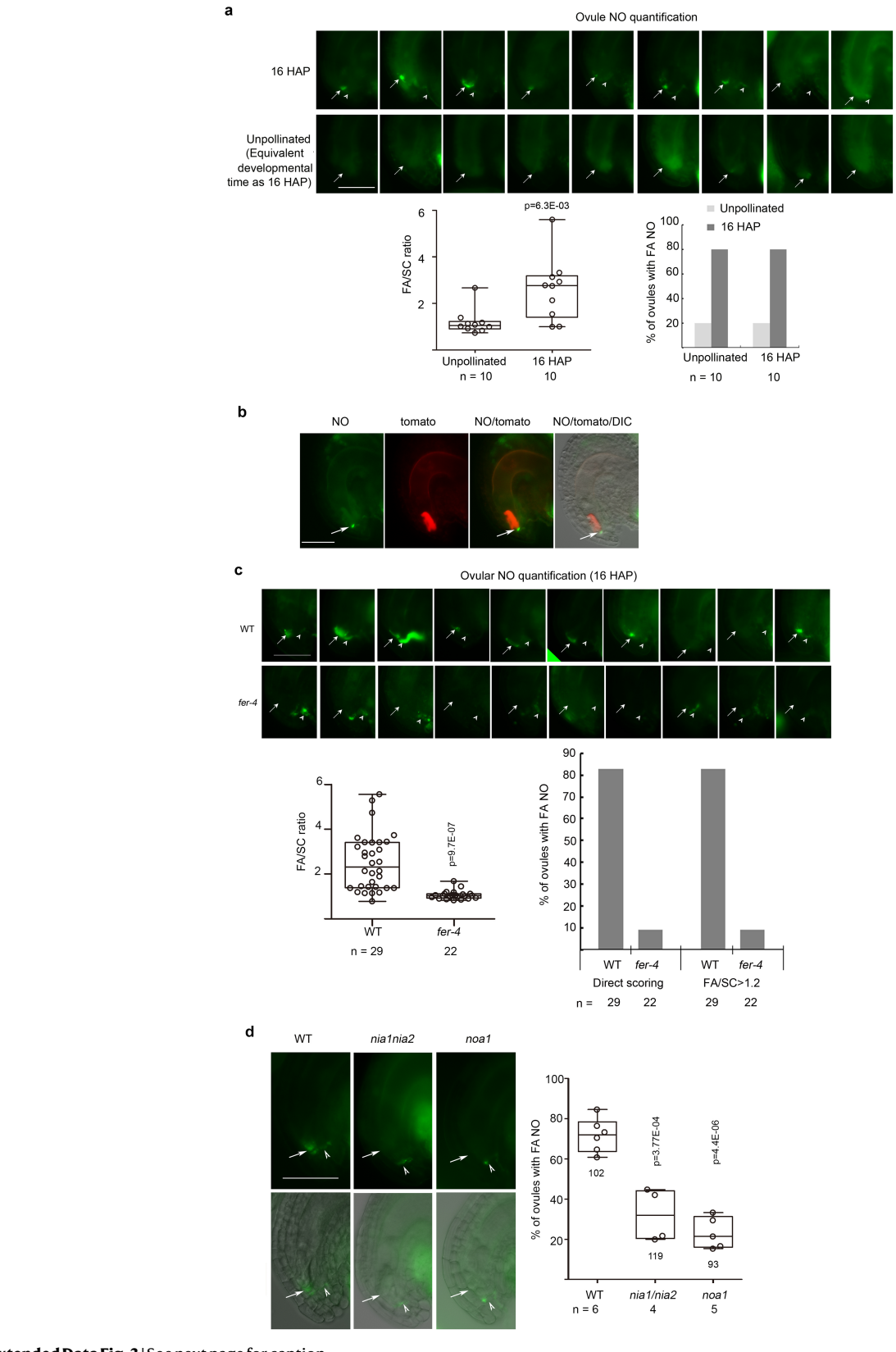
as it did the normal single pollen tube penetration phenotype (Extended Data Fig. 1c). ${f g}$, Quantification of de-esterified pectin located at the filiform apparatus by JIM5 and M38 signal levels, following a previously described method⁴. Average signal intensity in equal areas of interest (dotted lines) at the filiform apparatus and in the synergid cells were compared. A filiform apparatus:synergid cell ratio of ≥1.2 was scored as JIM5- or M38-positive. h, JIM7 immunostaining of ovule methylesterified pectin. Arrows, filiform apparatus region. Image acquisition conditions were the same as those for JIM5 immunostaining (Fig. 1e). Signal was below detection, most probably because of the high solubility of the methylesterified polymers during the immunostaining procedure, which involved extensive washes. i, JIM5 immunostaining of wild-type and FERp::PMEI1-GFP (PMEI1ox) ovules. Overexpression of PMEI1 (Extended Data Fig. 2) reduced the localization of deesterified pectin at the filiform apparatus. i, M38 immunostaining of wild-type, pme44, pme34 and PMEIox ovules. Reduced M38 and JIM5 signals correlated with augmented multiple pollen tube entry phenotype (Fig. 1g). Data shown are average \pm s.d. n, pistil numbers (\mathbf{c} , \mathbf{e} , \mathbf{f} , \mathbf{h} - \mathbf{j}); n, ovule numbers (\mathbf{g}). Data are $representative of three independent \, experiments. \textit{P} \, values \, were \, obtained \, bv \, and \, bv \, and \, bv \, are a constant of the property of the proper$ two-tailed t-tests; numbers in data plots represent the number of ovules examined. Scale bar, 1 mm (a), 50 μm (d, g, h). Box plots: centre line, median; box limits, lower and upper quartiles; dots, individual data points; whiskers, highest and lowest data points.



Extended Data Fig. 2 | See next page for caption.

Extended Data Fig. 2 | Characterization of mutants deficient in de-esterified pectin. a-d, Transfer (T-) DNA insertion mutants pme34-1 (Salk_062058)30 and pme44-1 (SALK 071362). a, c, Genomic maps with T-DNA insertions (triangles). **b**, **d**, PCR with reverse transcription for *PME34* and *PME44* mRNAs from seedlings (S) and flowers (F). Green arrows, primers for RT-PCR; black and red arrow pairs, primers for genotyping. e-g, Flowering wild-type, pme34-1, pme44-1 and PMEI1ox plants. Growth, flowering time, flower morphology and reproductive yields (silique sizes, arrows in f, g, and seed numbers) of these transgenic mutant plants were adequately normal relative to wild type, permitting reproductive studies. h-k, FERp::PMEI1-GFP expression and ovule morphology in PMEI1ox plants. PMEI1-GFP expression in seedlings and ovules paralleled that of FERp::FER-GFP^{4,10}, including a most-prominent accumulation in the elongation zone of seedling roots (h), throughout the ovules and prominently at the filiform apparatus region (arrowheads) (i). Ovules appeared mostly normal, although higher level of autofluorescence was observed in the sporophytic tissue of some ovules (white arrows). When stained by aniline blue, most ovules from the plants used here appeared normal (j). Some ovules showed elevated callose deposition in the sporophytic as well as in the female

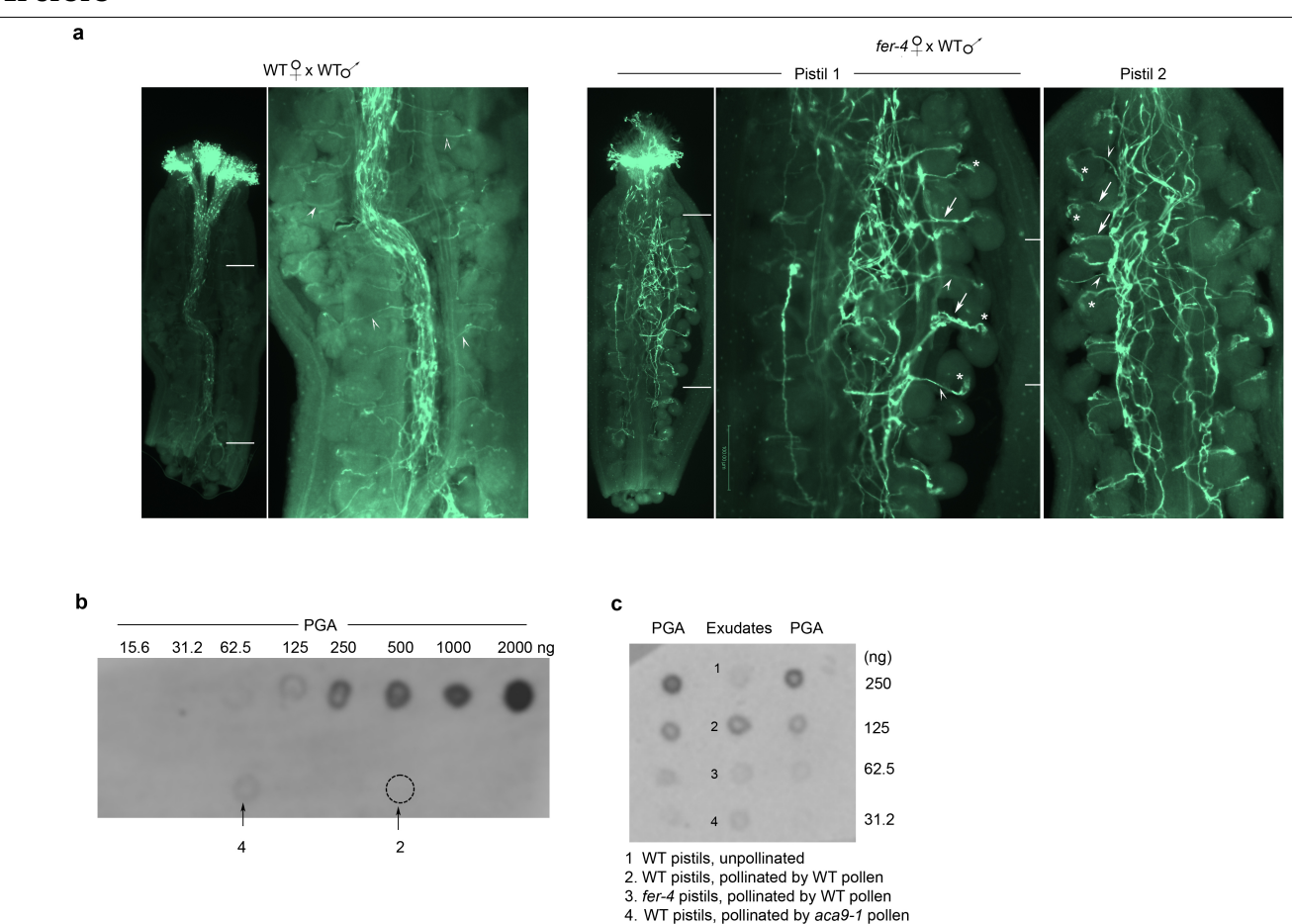
gametophyte region (k), reflecting stress. Ovules with overaccumulation of callose are generally not penetrated by pollen tubes, so were excluded from these studies. Extended Data Figure 10a-c shows defects in a PMEI5overexpression line²⁰, precluding its use in these studies. I, Statistical comparison among mutants deficient in de-esterified pectin and transgenic plants. The levels of ovules penetrated by multiple pollen tubes in pme34, pme44 and PMEI1ox plants were not significantly different among them (bracket 1). Deficiency in de-esterified pectin among these mutant ovules was also not significantly different (Extended Data Fig. 1j). Attempts to compound their effect in a pme34 pme44 double mutant (arrowheads indicate a penetrating pollen tube doublet) did not result in a significantly higher multiple-tube penetration phenotype than the single mutant parents (bracket 2). Data for pme34, pme44 and PMEIIox plants were from Fig. 1g. Data for pme44 and pme34 are average ± s.d. n, number of pistils. Results were representative of three independent experiments. P values were obtained by two-tailed t-tests; numbers in data plots denote the number of ovules examined. Box plots: centre line, median; box limits, lower and upper quartiles; dots, individual data points; whiskers, highest and lowest data points.



Extended Data Fig. 3 | See next page for caption.

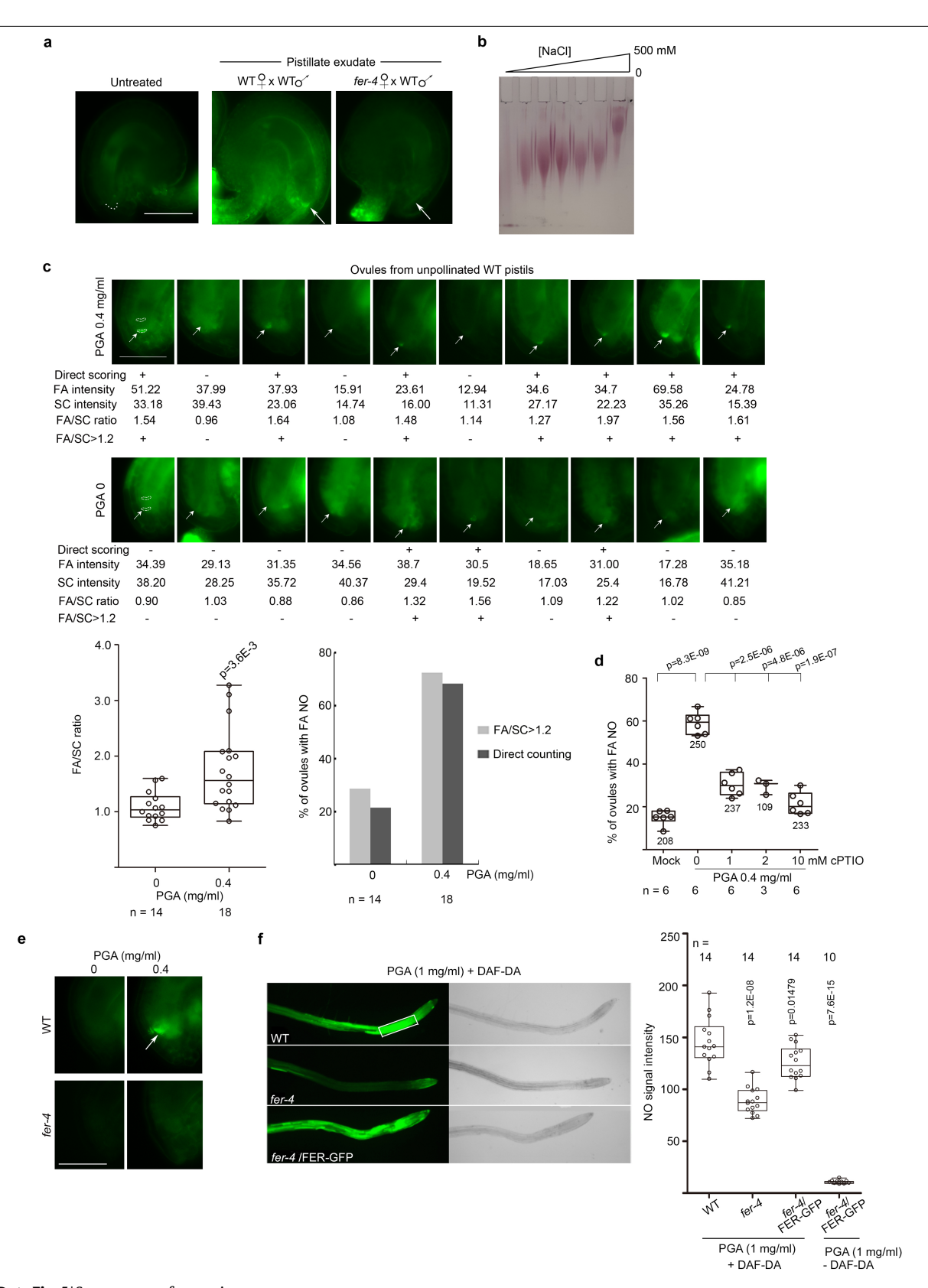
Extended Data Fig. 3 | Ovular NO status in wild type and NO-deficient mutants. a, Comparison of two methods of ovule NO quantification. Ovules from pollinated (16 h after pollination) and unpollinated wild-type pistils at the same developmental stage were examined. Images were acquired with identical conditions and a sampling of ovules is shown. In the direct scoring method, ovules were scored as positive (+) when signal at the filliform apparatus (arrow, filliform apparatus) was notably higher than in the synergid cell (right histogram). In the filliform-apparatus/synergid-cell signal-intensity-ratio method, average signal intensity of identical areas at the filliform apparatus and in the synergid cell (as background) was determined by ImageJ. A filliform apparatus synergid cell ratio of ≥1.2 was scored as + (left dot plot). The two methods gave comparable conclusions. Data are average ±s.d. *n*, number of ovules. *P* values were obtained by two-tailed *t*-tests. **b**, Full ovule images for

Fig. 2b. The ejected pollen cytoplasm (red) marked the synergid cell, providing a clear spatial definition for NO located at the filiform apparatus (arrow). **c**, Comparison of filiform apparatus: synergid cell NO signal intensity in pollinated wild-type and *fer-4* ovules (left dot plot) and direct scoring (right histogram). Results were comparable. Data (left dot plot) are average \pm s.d. *n*, number of ovules. **d**, NO in wild-type, *nia1 nia2* and *noa1* mutant ovules. The results correlated reduced filiform-apparatus NO in these pollen-tube-penetrated ovules with elevated multiple pollen tube entrance (Fig. 2e). Data are average \pm s.d. *n*, number of pistils. Numbers in plot denote the number of ovules examined. *P* values were obtained by two-tailed *t*-tests. Data are representative of three independent experiments. Scale bars, 50 µm. Box plots: centre line, median; box limits, lower and upper quartiles; dots, individual data points; whiskers, highest and lowest data points.



Extended Data Fig. 4 | Quantification of pollinated pistil exudate.

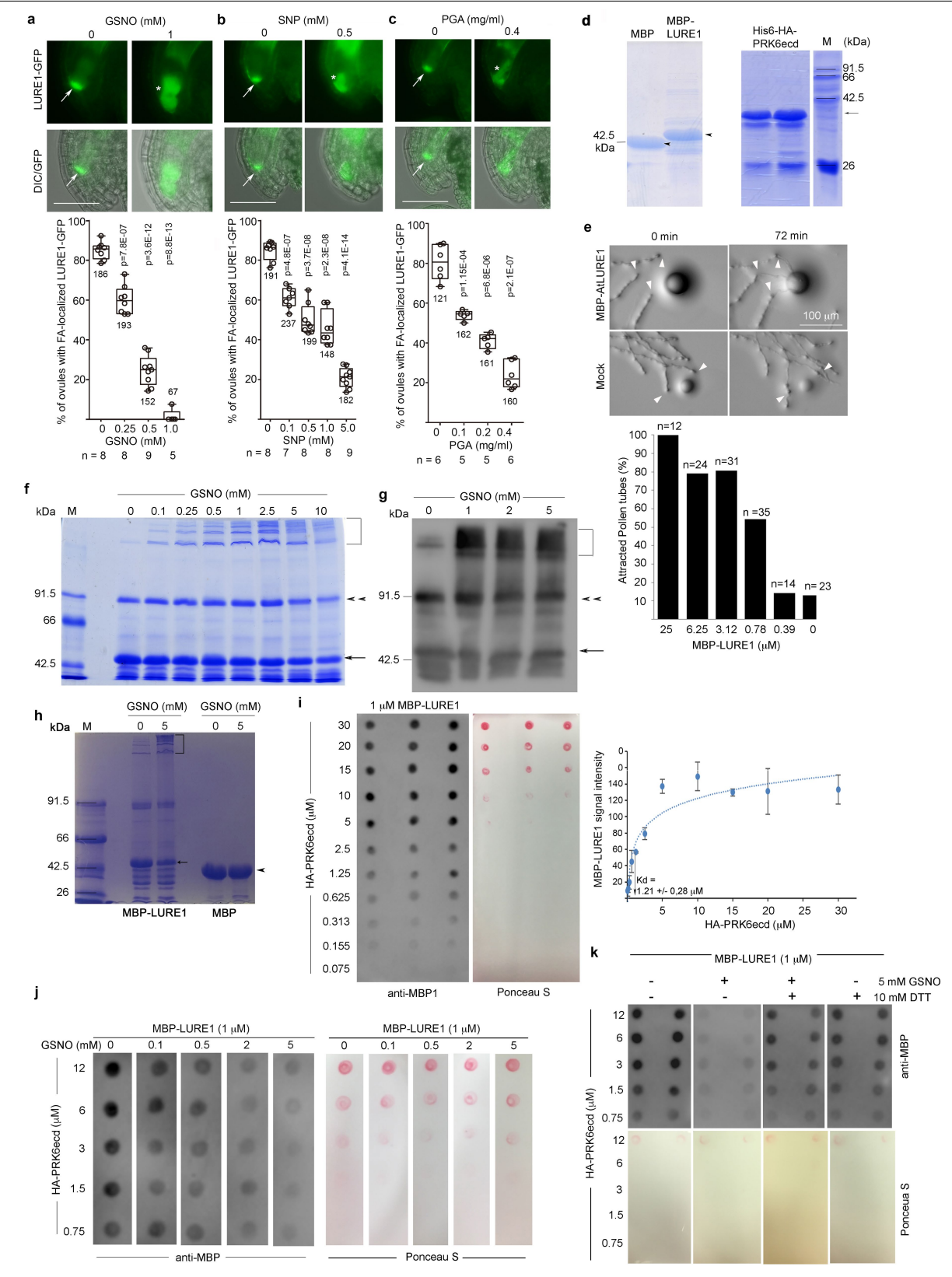
as indicated. Two microlitres—equivalent to exudates from 10 pistils—was spotted on filter; PGA dots were prepared as described in **b** for dot blot quantification. JIM5 was used for immunodetection. Only exudate 2, from pollinated wild-type pistils, showed a notable level of JIM5-detected deesterified pectin, approximating 125 ng (about 12.5 ng per pistil). A low level of JIM5 signal in sample 4 correlated with few $aca9\cdot 1$ pollen tubes in the pollinated pistils (Extended Data Fig. 10d, e). Four microlitres (that is, about 250 ng of JIM5-detected materials) of similarly prepared exudates was applied to ovule NO assays (Fig. 3b). On the basis of pistil dry weight (32 μ g per pistil, averaged from batches of 25 dried pistils from flowers around stage 14), the pistillate exudate JIM5-detectable material recovery would be about 0.04%. These quantifications were, however, approximations; precise quantification of these reagents will need substantial further refinement.



Extended Data Fig. 5 | See next page for caption.

Extended Data Fig. 5 | De-esterified pectin induces FER-dependent NO production. a, Exudates from pollinated wild-type, but not fer-4, pistils induced NO at the filiform apparatus region (arrows) of wild-type ovules. b, Sonicated PGA ($100 \mu g$) electrophoresed in a 26% polyacrylamide gel 47 . Lanes represent fractions eluted from a diethylaminoethyl column by the indicated salt gradient. The last fraction approximated PGA before sonication. Oligogalacturonic-acid-sized 25 fragments would be ahead of the RuR-stained materials on the basis of comparison with a previous publication 47 . Active species for ovular NO induction remains to be determined. c, Representative quantification of PGA-induced NO response based on filiform apparatus:synergid cell signal ratio, as described in Extended Data Fig. 3a. Data plots summarize the quantification data (left dot plot) and data from direct scoring (right histogram), showing comparable results. Data are average \pm s.d.,

n, number of ovules. \mathbf{d} , cPTIO suppressed PGA induced accumulation of NO at the filiform apparatus. cPTIO was added together with the DAF-DA dye. Data are average \pm s.d. n, number of pistils. \mathbf{e} , PGA treatment of wild-type and fer-4 ovules showed NO in wild-type (arrow), but not fer-4, filiform apparatus. \mathbf{f} , PGA treatment of wild-type, fer-4 and FER-GFP-complemented fer-4 seedling roots showed FER dependence for PGA-induced root NO. Under equal image acquisition conditions (but without added DAF-DA), FER-GFP signal was negligible (last data bar). Signals were quantified from equal areas of interest (white box). Data are average \pm s.d., n, number of seedlings. P values were obtained by two-tailed t-tests. Scale bars, 50 μ m. All observations were representative of three independent experiments. Box plots: centre line, median; box limits, lower and upper quartiles; dots, individual data points; whiskers, highest and lowest data points.

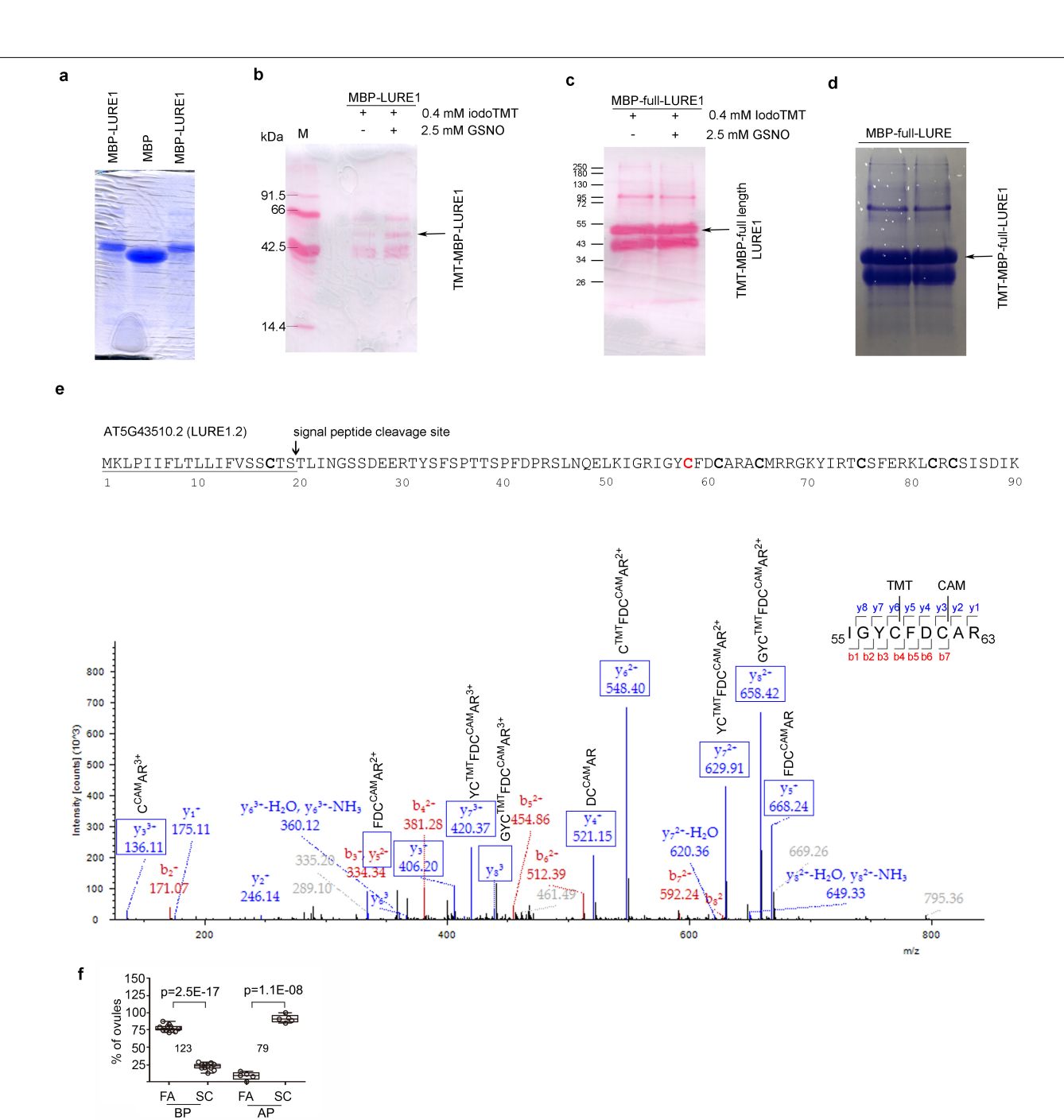


Extended Data Fig. 6 | See next page for caption.

Extended Data Fig. 6 | Effect of pectic fragments and NO on LURE1

properties. a-c, Wide-field images of control, GSNO-, SNP- and PGA-treated LURE1-GFP-expressing ovules from unpollinated pistils. Data are average \pm s.d. n, number of pistils. Representative of three independent experiments. P values were obtained by two-tailed t-tests; numbers in plots denote the number of ovules examined. d, SDS-PAGE of purified E.-coli-produced MBP, MBP-LURE1 (arrowheads) and the extracellular domain of its receptor PRK6 (His₆-HA-PRK6(ecd)) (arrow). M, molecular mass markers. e, MBP-LURE1 attracts pollen tubes. Top, purified MBP-LURE1 was used in pollen tube attraction assays^{1,37} in semi-pollen tube growth cultures. Arrowheads, tips of pollen tubes at the time of bead application. Bottom, histogram shows MBP-LURE1 dose-dependent pollen-tube-attraction activity. Attraction efficiency was similar to that in a previous study¹. Mock treatment (0) used MBP in gelatin beads. Scale bars, 100 µm. Data are representative of multiple independent protein preparations using a similar range of MBP-LURE1 concentrations. f-h, GSNO treatment of MBP-LURE1. f, MBP-LURE1 was mock-treated or incubated with GSNO before application for SDS-PAGE in the absence of β-mercaptoethanol, followed by Coomassie-blue staining. g, An immunoblot by anti-MBP antibody of an experiment similar to that in f. Arrow, double arrowheads and bracket indicate monomeric MBP-LURE1, dimer-sized and higher-molecular-weight forms, respectively. h, Comparison of GSNO treatment of MBP and MBP-LURE1 shows no notable effect on the molecular weight of MBP. Collectively comparable observations were made in at least six

independent experiments. i, j, Dot blot assay for LURE1 interaction with its receptor PRK6 26,27 . i, Equal volumes (1.5 μ l) of increasing concentrations of HA-PRK6(ecd) were applied to filter in triplicate rows for interaction with MBP-LURE1, then processed for immunodetection of bound MBP-LURE1 by anti-MBP antibody. Ponceau-S-stained filter illustrates quantitative spotting of HA-PRK(ecd) to the membrane. Data plot (right) shows signal intensity from the bound MBP-LURE1. Data are averaged from the triplicate binding samples \pm s.d., showing a K_d of about $1.21\pm0.28\,\mu\text{M}$, approximating the previously reported affinity²⁶. j, Dot blot assay for PRK6(ecd) interaction with control (0) and MBP-LURE1 treated with increasing concentration of GSNO. PRK6(ecd) on membrane was incubated with MBP-LURE1, and the interaction was detected by anti-MBP. Ponceau-S-stained filters confirmed quantitative spotting of PRK6(ecd). The result from the 12-µg bait blots (top row) is shown in Fig. 4c. k, Effect of DTT on GSNO-induced inhibition of MBP-LURE1 binding to HA-PRK6(ecd). MBP-LURE1 was preincubated with combinations of DTT and GSNO as shown, before application to an HA-PRK6(ecd) filter for binding. filters. Results indicate reducing conditions mitigated GSNO inhibition. Collectively, similar observations were made in three independent experiments (i, j) or two for k; the triplicated and duplicated dots in i, k served as technical replicates. Box plots: centre line, median; box limits, lower and upper quartiles; dots, individual data points; whiskers, highest and lowest data points.



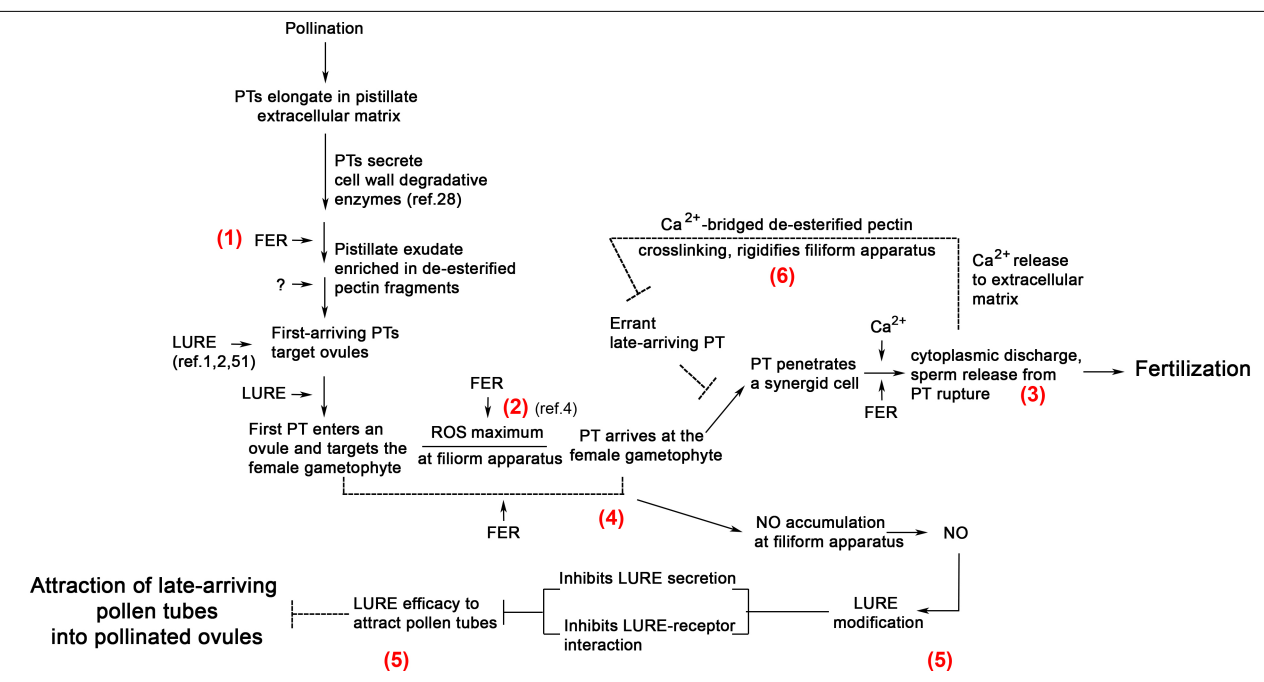
Extended Data Fig. 7 | **Analysis of LURE1 nitrosation. a**, Coomassie-blue-stained gel of typical MBP and MBP-LURE1 preparations used for nitrosation assays. **b**, Ponceau-S-stained protein blot for detection of TMT-labelled MBP-LURE1 (arrow); immunoblot is shown in Fig. 4e. **c**, Ponceau-S-stained protein blot for detection of TMT-labelled MBP-full-length LURE1 (arrow); immunoblot is shown in Fig. 4e. **d**, Coomassie blue-stained purified MBP-full-length LURE1 after TMT-labelling reaction (arrow). The recombinant protein with LURE1 signal peptide tended to break down during the labelling procedure, producing a lower band at the MBP molecular weight range. The MBP-full LURE1 protein bands indicated by the arrow were excised for mass

n = 11

spectrometry analysis shown in Fig. 4e, g, h. e, LC-MS/MS spectrum showing TMT-Cys58-containing peptides, and LURE1.2 amino acid sequence highlighting Cys58. f, LURE1p::LURE1-GFP localization in ovules from unpollinated (BP) or pollinated (AP) pistils for comparison with LURE1(C17A)-GFP localization (shown in Fig. 4i). As shown in Fig. 4a, LURE1-GFP typically located in the filiform apparatus in ovules from unpollinated pistils, and delocalized to the cytoplasm of synergid cells in ovules from pollinated pistils. Box plots: centre line, median; box limits, lower and upper quartiles; dots, individual data points; whiskers, highest and lowest data points.

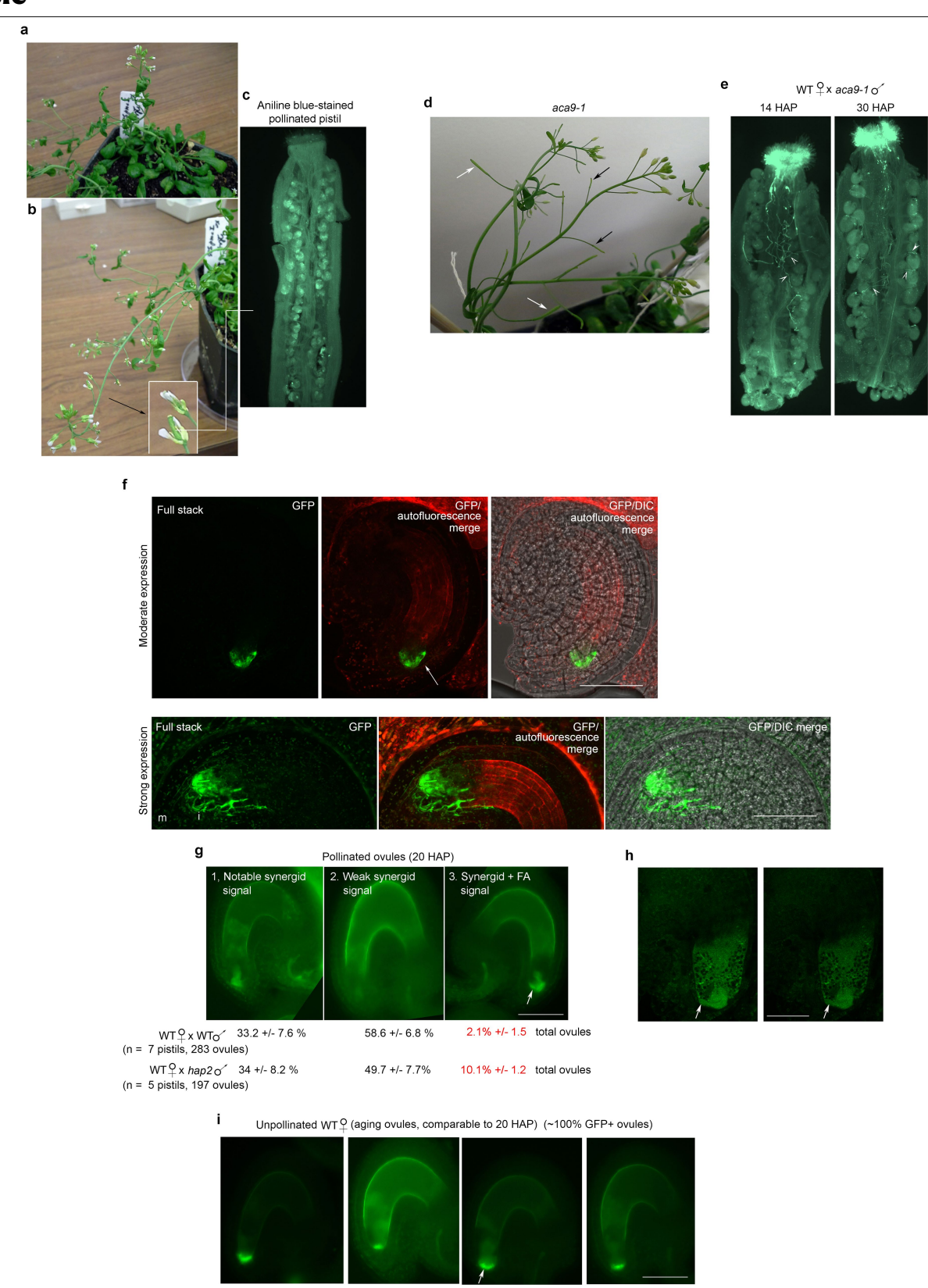
AtLURE1.1 AtLURE1.2 AtLURE1.3 91 AtLURE1.4 90 AtLURE1.5 90 AtLURE1.7 93 AtLURE1.8 93 XIUOIU1 101 XIUQIU2 XIUQIU3 MKTIFFF-ITFIVLVSSETSNIMTKSISQVKSQFFSPALSPNVDPAD------EHIGHSPDDMKIIFCQQCAFHCIEKKK--NIGNC--ENSICRETLEDI-----L XIUQIU4

 $\textbf{Extended Data Fig. 8} | \textbf{Sequence alignment.} Sequence alignment of full-length LURE1s^1 and LURE1-related XIUQIUs^2.$



Extended Data Fig. 9 | A summary of FER-regulated pollen tube-ovule interaction. The diagram summarizes previously published results on how FER mediates pollen tube rupture and sperm release to enable fertilization⁴ (steps 2 and 3 in the scheme), and results reported here on how FER affects two interconnected conditions at the filiform apparatus to prevent the penetration of ovules by supernumerary pollen tubes (steps 4 and 5 in the scheme). Solid lines reflect information that comes directly from experimental data; dashed lines reflect extrapolations from experimental data and other relevant information. Results present in this Article show that FER maintains a pistillate environment enriched in de-esterified pectin (Fig. 3a) (step 1 in the scheme), including at the filiform apparatus of the female gametophyte (Fig. 1e, f). Pollen tubes are attracted by female guidance cues to depart from their main growth axis to approach ovules, and are then guided by synergid-cell-produced chemoattractants (for example, LUREs) to the ovules to penetrate the female gametophyte^{1,5,6} (Fig. 1b,c, Extended Data Fig. 1b). In penetrating the filiform apparatus that is enriched in de-esterified pectin, the pollen tube that arrives first should continue to secrete cell-wall degradative enzymes-presumably producing pectic fragments in the vicinity, just as growth in the transmitting track produced these polymers (Fig. 3a, Extended Data Fig. 4). The application of pollinated pistillate exudate enriched in de-esterified pectin (Fig. 3b) and

fragmented, commercially obtained de-esterified pectin (Fig. 3c, d) to ovules from unpollinated pistils, and the arrival of pollen tubes at ovules in pollinated pistils (Fig. 2a, b) (step 4 in the scheme), triggered NO accumulation at the filiform apparatus. Taken together with the observation that NO-deficient ovules also had elevated levels of multiple pollen tube entrance (Fig. 2e), these results are consistent with pectic fragments generated by pollen tube growth acting as a mediator to trigger NO accumulation to prevent the entrance of supernumerary pollen tubes (step 4 in the scheme). Our results demonstrate that NO does so by modifying LURE and disengaging LURE-mediated attraction of late-arriving pollen tubes to already penetrated ovules (steps 4 and 5 in the scheme) (Fig. 4, Extended Data Figs. 6, 7). Previously published results⁴, and the properties of de-esterified pectin, are consistent with an altered ovular environment before and after pollen tube rupture. This could be achieved (for example) by Ca²⁺ leakage from the degenerating synergid cell and Ca²⁺ released from the ruptured pollen tube. The elevated extracellular [Ca2+] would immediately mediate stiffening of the filiform apparatus that is rich in deesterified pectin. The stiffened cell wall could then present a back-up blockade to prevent entrance by an errant, late-arriving pollen tube into an already penetrated female gametophyte (step 6 in the scheme).



Extended Data Fig. 10 | See next page for caption.

Extended Data Fig. 10 | Additional considerations. a-c, CaMV35S::PMEI5-transformed plants are severely compromised in female fertility.

a, Constitutive expression of PMEI5 severely affected plant development²⁰. b, Flower organogenesis appeared normal, but pistil development was suppressed; at maturity, pistils were at most 1/3 of the normal size. Pollen production appeared normal. c, The stigmatic papillae of these plants were under-developed; pollinated stigma did not retain any pollen grains, reflecting their inability to support pollen germination to penetrate the stigmatic papillae. The aniline blue-stained ovules showed high levels of callose deposition, a symptom of stress. Even in normal pistils, ovules with ectopic callose accumulation do not attract pollen tubes (Extended Data Fig. 2j, k), precluding these PMEI5-overexpressing ovules from being used in ovule penetration studies. Very few seeds were produced from these PMEI5overexpressing plants (about 10 µl of seeds from a full pot was a good yield under our growth condition). Similar observations were made in several plantings, as we obtained the seeds in 2014.d, e, aca9-1 pollinated pistils. **d**, Flowering aca9-1 plants produced many under-developed siliques (black); even elongated siliques (white arrows) had a substantially reduced number of fertilized ovules 40. e, aca 9-1 pollination of wild-type pistils. Aniline blue staining showed few elongating pollen tubes and their arrival at ovules (arrowheads), even at 30 h after pollination. Exudates from pistils pollinated by aca9-1 pollen showed a basal level of de-esterified pectin (Extended Data Fig. 4c). These observations are linked to the experiment presented in Extended Data Fig. 4; together, four independent preparations showed comparable results. f-i, NO as a gaseous agent to block the entrance of supernumerary pollen tubes. Observations below are included here to relate how findings from the present study might be linked to several topics that are not yet fully understood. f, Confocal images of mature ovules from unpollinated pistils expressing a moderate level of LURE1-GFP (top; a large majority of ovules in the transformed pistils), showing the typical filiformapparatus (arrow) localization. Occasionally, an ovule overexpressed LURE1-GFP (bottom), showing the presence of the protein in the inner integuments (i) that envelope the micropylar (m) chamber. The working distance of the LURE1 gradient diffused from the filiform apparatus is not known, although histoimmunodetection suggests that it reaches the micropylar region¹. NO, as

a gaseous molecule, should diffuse readily and reach the micropylar region (and possibly beyond), although its working distance is unknown and difficult to determine. These observations are included for the consideration of plausible functional linkage between the two gradients that would be expected to exist in the system. ${f g}$, LURE1-GFP localization at completion of pollination (20 h after pollination) in LURE1p::LURE1-GFP pistils by wild-type pollen. Typically fewer than 50% of the ovules showed notable GFP signal in the synergid cell (category 1) (Fig. 4a, b); others retained a weak synergid cell signal (category 2). A low percentage of ovules showed LURE1-GFP localization in both the filiform apparatus (arrow) and the synergid cell (category 3). When pollinated by pollen from hap 2/+ mutant plant, the sperm from half of the applied pollen (hap2 pollen) was incompetent for fusion; therefore, half of the ovules were not fertilized12. A higher percentage of ovules from hap2/+ pollinated pistils showed category-3 localization, with notable synergid cell as well as filiform apparatus LURE1-GFP signal. h, Confocal image of a category-3 ovule. A maximum projection from 4 images (1 µm total thickness) (left) and a $single\ optical\ section\ (right), showing\ LURE1-GFP\ localization\ in\ a\ synergid\ cell$ and across the filiform apparatus. It could be envisioned that category 3 oyules in hap2/+ pollinated pistils could be candidates for fertilization recovery (that is, having the propensity to salvage fertilization). In the hours after failed fertilization, NO induced by the arrival of the sterile hap2 pollentube could have dissipated (for example, see data plot in Fig. 2c), allowing some level of secretion of newly synthesized LURE1 and pollen tube attraction to be reactivated. The phenomenon in g was observed in every experiment reported in Fig. 4a (leftmost two panels). The data presented here were pooled from two independent experiments, designated to collect the numerical data presented $here for discussion. \textbf{\textit{i}}, Unpollinated but ageing ovules maintained LURE1-GFP$ at their filiform apparatus and thus should continue to be competent in pollen tube attraction. These data also demonstrate that NO accumulation at the filiform apparatus does not correlate with ovule age, providing further support for the notion that NO accumulates in response to pollen tube arrival. These observations were similar to those in Fig. 4a (left) and control experiments shown in Extended Data Fig. 6a-c. Scale bars, 50 μ m. Arrows, filiform apparatus region.



Corresponding author(s): Alice Cheung, Hen-Ming Wu

Reporting Summary

Nature Research wishes to improve the reproducibility of the work that we publish. This form provides structure for consistency and transparency in reporting. For further information on Nature Research policies, see <u>Authors & Referees</u> and the <u>Editorial Policy Checklist</u>.

Statistical parameters

		atistical analyses are reported, confirm that the following items are present in the relevant location (e.g. figure legend, table legend, main Methods section).
n/a	a Confirmed	
	\boxtimes	The $\underline{\text{exact sample size}}(n)$ for each experimental group/condition, given as a discrete number and unit of measurement
	\boxtimes	An indication of whether measurements were taken from distinct samples or whether the same sample was measured repeatedly
	\boxtimes	The statistical test(s) used AND whether they are one- or two-sided Only common tests should be described solely by name; describe more complex techniques in the Methods section.
\boxtimes		A description of all covariates tested
\times		A description of any assumptions or corrections, such as tests of normality and adjustment for multiple comparisons
\boxtimes		A full description of the statistics including <u>central tendency</u> (e.g. means) or other basic estimates (e.g. regression coefficient) AND <u>variation</u> (e.g. standard deviation) or associated <u>estimates of uncertainty</u> (e.g. confidence intervals)
\boxtimes		For null hypothesis testing, the test statistic (e.g. <i>F</i> , <i>t</i> , <i>r</i>) with confidence intervals, effect sizes, degrees of freedom and <i>P</i> value noted <i>Give P values as exact values whenever suitable.</i>
\times		For Bayesian analysis, information on the choice of priors and Markov chain Monte Carlo settings
\times		For hierarchical and complex designs, identification of the appropriate level for tests and full reporting of outcomes
\boxtimes		Estimates of effect sizes (e.g. Cohen's d, Pearson's r), indicating how they were calculated
	\boxtimes	Clearly defined error bars State explicitly what error bars represent (e.g. SD, SE, CI)

Our web collection on <u>statistics for biologists</u> may be useful.

Software and code

Policy information about <u>availability of computer code</u>

Data collection no commercial or custom code used for this study

Data analysis no commercial or custom code used for this study

For manuscripts utilizing custom algorithms or software that are central to the research but not yet described in published literature, software must be made available to editors/reviewers upon request. We strongly encourage code deposition in a community repository (e.g. GitHub). See the Nature Research guidelines for submitting code & software for further information.

Data

Policy information about <u>availability of data</u>

All manuscripts must include a data availability statement. This statement should provide the following information, where applicable:

- Accession codes, unique identifiers, or web links for publicly available datasets
- A list of figures that have associated raw data
- A description of any restrictions on data availability

The data sets generated during and/or analyzed during the current study are available from the corresponding author on reasonable request.

Field-specific reporting				
Please select the best fit for your research. If you are not sure, read the appropriate sections before making your selection.				
Life sciences Behavioural & social sciences Ecological, evolutionary & environmental sciences				
For a reference copy of the document with all sections, see <u>nature.com/authors/policies/ReportingSummary-flat.pdf</u>				
Life sciences study design				
Life sciences study design				
All studies must disclose on these points even when the disclosure is negative.				
Sample size Sampling was from pistils (the entire female organ), about 20-30 undamaged ovules (the organ for fertilization) were scored per pistil. So n = 6-9 pistils for most experiments; for n < 6, the difference was significant and less variable. [Total # of ovules examined per assay wer also indicated in plots]. In Fig. 4d, n = samples of pollen tubes (the sperm-bearing male cell), each sample > 40 pollen tubes, per in vitro assay. [Total # of pollen tubes examined per assay were also indicated in plot). In Fig., 3e, Ext. Fig. 5f, n = number of roots per assay, sampling size >10 seedlings per assay.	е			
Statistics was by student T-Tests, two tailed.				
Data exclusions No data exclusion.				
Replication Data were from at least three independent replications per experiment. All data from replicates showed comparable trends. Some data sets were also replicated for different inquiry purposes, they showed similar trends also as when they were carried out for their own inquiry purpose.	S			
Randomization Samples from identifiable developmental stages were randomly picked.				
Data were from at least three independent replications per experiment. All data from replicates showed comparable trends. Some data sets were also replicated for different inquiry purposes, they showed similar trends also as when they were carried out for their own inquiry purpose. Data sets from initial efforts for each set of experiments were analyzed in two ways, one by experimenter, one blind by co-investigators to ensure comparable scoring. Some data sets were backed up from experiments independently carried out by one or more convergence experimenters, and over a period of time. Data were from at least three independent replications per experiment. All data from replicates showed comparable trends. Some data set were also replicated for different inquiry purposes, they showed similar trends also as when they were carried out for their own inquiry purpose.	0-			
Paparting for specific materials, systems and methods				
Reporting for specific materials, systems and methods				
Materials & experimental systems Methods				
n/a Involved in the study n/a Involved in the study				
Unique biological materials ChIP-seq Antibodies Flow cytometry				
Eukaryotic cell lines MRI-based neuroimaging				
Palaeontology				
Animals and other organisms				
Human research participants				
Unique biological materials				
Policy information about <u>availability of materials</u>				

Obtaining unique materials No restrictions

Antibodies

Antibodies used

Pectin antibodies, JIM5, JIM7, M38 are from Complex Carbohydrate Research Center; JIM5, catalog CCRC-JIM5 (EG.C6) diltution 1:500

JIM7, catalog CCRC-JIM7 (no lot #), dilution 1:50 M38, catalog CCRC-M38 (no lot #), dilution 1:50

anti TMT from ThermoFisher ,Cat# 90075 (provided as part of Cat# 90105 labeling kit) (Lot DH190916), dilution: 1:1000 anti-MBP antibody (NEBL),E8038S, lot 0111607, dilution 1:20000

Secondary antibodies were from commercial sources:

goat anti-rat IgG-FITC conjugated, Santa Cruz (sc2011), Lot H2312, L1709.; dilution 1:100. goat anti-mouse IgG-FITC conjugated, Santa Cruz (Sc2010); diution 1:100.

Anti HA-HRP, Santa Cruz, Cat. 7392, lot A0318, dilution 1:2000 Goat anti-mouse-HRP, Aesar, Cat # J64787, Lot 5740203; dilution 1:2000.

Validation

JIM5, JIM7 and M38 were established monoclonal antibodies used extensively in plant cell wall research. The lots used in this study should have been validated by supplier and others in the literature, and confirmed by us in comparative studies between wild type and pectin-deficient mutants.

All other secondary antibodies should have been validated by producers, and confirmed by by us in comparative immunoblots using proteins from wild type and plants expressing the corresponding tagged-protein.

Animals and other organisms

Policy information about studies involving animals; ARRIVE guidelines recommended for reporting animal research

Laboratory animals

For laboratory animals, report species, strain, sex and age OR state that the study did not involve laboratory animals.

Wild animals

Provide details on animals observed in or captured in the field; report species, sex and age where possible. Describe how animals were caught and transported and what happened to captive animals after the study (if killed, explain why and describe method; if released, say where and when) OR state that the study did not involve wild animals.

Field-collected samples

For laboratory work with field-collected samples, describe all relevant parameters such as housing, maintenance, temperature, photoperiod and end-of-experiment protocol OR state that the study did not involve samples collected from the field.